

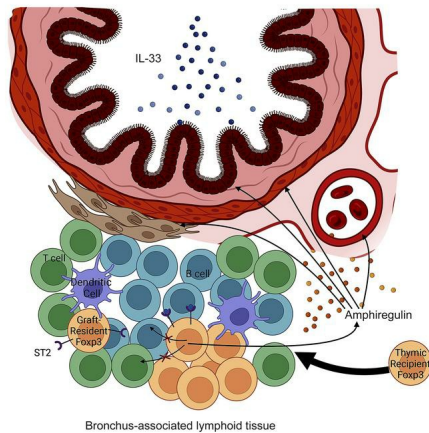
Maintenance of graft tissue-resident Foxp3^+ cells is necessary for lung transplant tolerance in mice

Wenjun Li, ... , Andrew E. Gelman, Daniel Kreisel

J Clin Invest. 2025. <https://doi.org/10.1172/JCI178975>.

Research In-Press Preview Immunology

Graphical abstract



Find the latest version:

<https://jci.me/178975/pdf>



**Maintenance of graft tissue-resident Foxp3⁺ cells is necessary for lung transplant tolerance
in mice**

Wenjun Li^{1,*}, Yuriko Terada^{1,*}, Yun Zhu Bai^{1,*}, Yuhei Yokoyama¹, Hailey M. Shepherd¹, Junedh M. Amrute², Amit. I. Bery², Zhiyi Liu¹, Jason M. Gauthier¹, Marina Terekhova³, Ankit Bharat⁴, Jon H. Ritter³, Varun Puri¹, Ramsey R. Hachem², Hēth R. Turnquist⁵, Peter T. Sage⁶, Alessandro Alessandrini⁷, Maxim N. Artyomov³, Kory J. Lavine^{2,3}, Ruben G. Nava¹, Alexander S. Krupnick⁸, Andrew E. Gelman^{1,3}, Daniel Kreisel^{1,3,§}

Affiliations: Departments of ¹Surgery, ²Medicine and ³Pathology & Immunology, Washington University in St. Louis, St. Louis, MO, ⁴Department of Surgery, Northwestern University, Chicago, IL, ⁵Department of Surgery, Starzl Transplantation Institute, University of Pittsburgh, Pittsburgh, PA, ⁶Transplantation Research Center, Renal Division, Brigham and Women's Hospital, Harvard Medical School, Boston, MA, ⁷Department of Surgery, Center for Transplantation Sciences, Massachusetts General Hospital, Boston, MA, ⁸Department of Surgery, University of Maryland, Baltimore, MD

*WL, YT and YZB contributed equally to this work

Corresponding Author:

Daniel Kreisel, MD, PhD

Department of Surgery, Washington University School of Medicine

660 South Euclid Avenue, Campus Box 8234, St. Louis, MO 63110

Tel: (314) 362-6021

Email: kreiseld@wustl.edu

Conflict-of-interest statement

The authors have declared that no conflicts of interest exist.

Abstract

Mechanisms that mediate allograft tolerance differ between organs. We have previously shown that Foxp3⁺ T cell-enriched bronchus-associated lymphoid tissue (BALT) is induced in tolerant murine lung allografts and that these Foxp3⁺ cells suppress alloimmune responses locally and systemically. Here, we demonstrated that Foxp3⁺ cells that reside in tolerant lung allografts differed phenotypically and transcriptionally from those in the periphery and were clonally expanded. Using a mouse lung re-transplant model, we showed that recipient Foxp3⁺ cells were continuously recruited to the BALT within tolerant allografts. We identified distinguishing features of graft-resident and newly recruited Foxp3⁺ cells and showed that graft-infiltrating Foxp3⁺ cells acquired transcriptional profiles resembling those of graft-resident Foxp3⁺ cells over time. Allografts underwent combined antibody-mediated rejection (AMR) and acute cellular rejection (ACR) when recruitment of recipient Foxp3⁺ cells was prevented. Finally, we showed that local administration of IL-33 could expand and activate allograft-resident Foxp3⁺ cells providing a platform for the design of tolerogenic therapies for lung transplant recipients. Our findings establish graft-resident Foxp3⁺ cells as critical orchestrators of lung transplant tolerance and highlight the need to develop lung-specific immunosuppression.

Introduction

Lung transplantation remains the only treatment option for many patients afflicted with end-stage pulmonary disease. However, outcomes after lung transplantation are poor compared to other solid organ transplants, with 5-year survival of about 60% (1). This is largely due the substantial proportion of patients developing chronic lung allograft dysfunction, which is a manifestation of chronic rejection. We have suggested that this high rate of graft failure is due to the clinical use of immunosuppressive agents that do not account for the unique immunological properties of lungs (2). For example, our group has described that several cell populations (e.g., memory CD8⁺ T cells, eosinophils) that can trigger rejection after the transplantation of other organs, may be critical for the downregulation of alloimmune responses after lung transplantation (3-5). Furthermore, while immune cell interactions in draining lymph nodes regulate graft acceptance after heart and pancreatic islet transplantation, we have shown that immune circuits that maintain tolerance after lung transplantation are established within the graft itself (6-9). Therefore, as immune pathways that regulate tolerance are not universal but rather organ-specific, a better understanding of mechanisms that mediate tolerance after lung transplantation represents an unmet need.

Our group has previously demonstrated that BALT, a tertiary lymphoid organ, is induced in tolerant lung allografts (7). Using a mouse lung re-transplant model, we have shown that Foxp3⁺ cells that accumulate within the BALT of tolerant lung allografts prevent the local activation of humoral immunity (6). Thus, graft tissue-resident Foxp3⁺ cells play a central role in lung transplant tolerance. Furthermore, pathogens which are known risk factors for lung allograft rejection can hinder the suppressive functions of Foxp3⁺ cells, raising the possibility that environmental stresses can disrupt tolerance after pulmonary transplantation (10). Therefore, it is important to define mechanisms that maintain a stable population of Foxp3⁺ cells within lung grafts.

In this study, we demonstrate that lung graft-resident Foxp3⁺ cells are phenotypically and transcriptionally distinct from Foxp3⁺ cells in the periphery of tolerant mice. Graft-resident Foxp3⁺ cells require ongoing replenishment by recipient-derived thymic Foxp3⁺ cells to maintain tolerance. Preventing the continuous recruitment of Foxp3⁺ cells triggers graft rejection with histological features of AMR and ACR. Finally, we explore a potential therapeutic approach to expand the graft-resident Foxp3⁺ cell population through local cytokine delivery.

Results

Allograft-resident and spleen Foxp3⁺ cells are phenotypically and transcriptionally distinct in tolerant lung transplant recipients

BALT develops in tolerant Balb/c lung allografts by 30 days after transplantation into C57BL/6 (B6) recipients that receive peri-operative costimulatory blockade (CSB) (Figures 1A,B) (7). The allografts had virtually no evidence of inflammation or cellular rejection and expression of club cell secretory protein (CCSP) was preserved in the airway epithelium of these grafts (Supplemental Figure 1; Figure 1C). We next performed allogeneic transplants from Balb/c donors into CSB-treated B6 CD11c-enhanced yellow fluorescent protein (EYFP)/Foxp3-green fluorescent protein (GFP) recipients followed by two-photon intravital imaging 30 days after engraftment (11). We noted that recipient Foxp3⁺ cells were predominantly located in close proximity to clusters of recipient CD11c⁺ antigen presenting cells which we and others have previously reported to reside in T cell zones of BALT (Figure 1D) (7, 12, 13). We then compared Foxp3⁺ cells that resided in tolerant lung allografts to Foxp3⁺ cells in the spleens of tolerant mice. We noted a higher abundance of Foxp3-expressing CD4⁺ T cells in lung allografts (Figure 1E). In addition, we observed lower levels of CD25 expression in graft-resident Foxp3⁺ cells, a shift towards an effector memory phenotype as well as higher expression levels of CD69 and PD-1 when compared to Foxp3 cells in the spleen (Figures 1F-I).

To investigate the gene expression patterns of Foxp3⁺ cells in lung grafts compared to those in the spleen, we next transplanted Balb/c lungs into B6 Foxp3-GFP recipients that were treated with perioperative CSB. Thirty days later CD4⁺ GFP⁺ cells were sorted from lung allografts and spleens and subjected to single-cell RNA sequencing. From these data, we synthesized an integrated dataset consisting of 946 and 727 tolerant lung and spleen Foxp3⁺ cells, respectively.

We examined the single-cell T cell receptor (TCR) profiles of graft- and spleen-resident Foxp3⁺ cells. Foxp3⁺ cells within grafts were more clonally expanded than those in the spleen (Figure 1J, left). While particular clonotypes were shared between both tissues, the most expanded ones were unique for the lung allograft tissue (Figure 1J, right). Differential gene analysis revealed markedly altered gene expression profiles in Foxp3⁺ cells in tolerant lungs compared to those isolated from spleens of tolerant recipients (Figure 1K). Of note, *Areg* (gene encoding amphiregulin), *Ctla4* and *Il1r1* (gene encoding ST2, the receptor for IL-33) were among the most highly differentially expressed genes in graft-resident Foxp3⁺ cells. To examine whether amphiregulin expression in Foxp3⁺ cells is functionally important, we next evaluated Balb/c lungs 30 days after transplantation into B6 recipients that lack *Areg* expression in Foxp3⁺ cells (Foxp3-YFP-Cre *Areg*^{fl/fl}). Compared to control conditions, these allografts were not ventilated, had neutrophilic capillaritis and alveolar inflammation, characteristic features of AMR, reduced expression of club cell secretory protein (CCSP) along with histological evidence of severe ACR (Figure 1L-N; Supplemental Figure 2). Amphiregulin is a ligand for the epidermal growth factor receptor (EGFR). To gain mechanistic insight how Foxp3⁺ cell-derived amphiregulin prevents allograft rejection, we transplanted Balb/c lungs into CSB-treated B6 Foxp3-YFP-Cre *Areg*^{fl/fl} mice or B6 Foxp3-YFP-Cre controls and examined allografts by single nuclear RNA sequencing 14 days later (Supplemental Figure 3A). We found that EGFR expression in the grafts was mostly restricted to stromal cells, including mesothelium, fibroblasts, smooth muscle cells and type II alveolar epithelium (Supplemental Figure 3B). Mesothelial cells harbored the largest number of differentially expressed genes between B6 Foxp3-YFP-Cre *Areg*^{fl/fl} recipients and controls (Supplemental Figure 3C). We identified two subtypes or states of mesothelial cells with a relative enrichment of the subtype that expresses *Col5a1*, *Col6a3*, *Col4a6*, and *Lum* after transplantation into mice that lack *Areg* in

Foxp3⁺ cells (Supplemental Figures 3D-F). We next examined transbronchial biopsies from human lung transplant patients, who had BALT with no evidence of ACR (Grade A0). In 4/5 of such biopsies we observed co-localization of staining for Foxp3 and amphiregulin (Supplemental Figure 4).

Graft-infiltrating Foxp3⁺ cells are derived from the thymus rather than from peripheral conversion of Foxp3⁻ T cells

We next examined the expression of Helios and Neuropilin-1 on Foxp3⁺ cells that reside in tolerant lung allografts at least 30 days after lung transplantation. These markers have been previously associated with thymic origin of regulatory T cells (14-16). Over 90% of graft-resident Foxp3⁺ cells expressed these markers (Figures 2A-C). To assess whether non-regulatory T cells convert into regulatory T cells within tolerant pulmonary allografts, we transplanted Balb/c (CD45.2) lungs into B6 (CD45.2) hosts that received peri-operative CSB. At least 30 days later we injected CD90⁺CD4⁺GFP⁻ T cells into these recipients that were isolated from spleen and lymph nodes of congenic (CD45.1) B6 Foxp3-GFP reporter mice. While we were able to detect adoptively transferred CD45.1⁺CD90⁺CD4⁺ T cells in tolerant lung allografts seven days after injection, they expressed virtually no GFP (Figures 2D,E). Collectively, these data indicate that Foxp3⁺ cells within tolerant lung allografts are derived from the thymus rather than from peripheral conversion of non-regulatory T cells.

Newly recruited Foxp3⁺ cells infiltrate BALT within tolerant lung allografts and differ transcriptionally from graft-resident Foxp3⁺ cells

We previously reported that tolerant lung allografts maintain a tolerant state after being re-transplanted into non-immunosuppressed recipients (6, 7, 17). Importantly, the re-transplant model allows us to distinguish between graft-resident and graft-infiltrating cells using congenic or fluorescent markers. To evaluate recruitment patterns of Foxp3⁺ cells that infiltrate tolerant lung allografts, we transplanted Balb/c lungs into B6 CD11c-EYFP recipients that were treated with peri-operative CSB. At least 30 days later we re-transplanted these lung allografts into non-immunosuppressed B6 Foxp3-GFP secondary recipients and performed intravital microscopy three days later. We found that recipient-derived graft-infiltrating Foxp3⁺ cells predominantly infiltrated BALT, hallmarked by CD11c⁺ cell aggregates, where they made close contact with these CD11c⁺ cells (Figure 3A; Supplemental Video 1). Moreover, in re-transplants of Balb/c lungs with CSB-treated B6 Foxp3-IRES-GFP primary recipients and non-immunosuppressed B6 Foxp3-IRES-red fluorescent protein (RFP) secondary recipients, we observed that graft-infiltrating Foxp3⁺ (RFP) cells also interacted with graft-resident Foxp3⁺ (GFP) cells (Figure 3B; Supplemental Video 2).

To compare gene expression profiles of graft-resident with newly recruited Foxp3⁺ cells we transplanted Balb/c (CD45.2) lungs into B6 (CD45.2) mice that received peri-operative CSB and re-transplanted these allografts into non-immunosuppressed B6 (CD45.1) recipients at least 30 days later. Seven and 21 days after re-transplantation, we obtained single-cell RNA sequencing data of sorted CD45.2⁺ and CD45.1⁺ cells from lung allografts. We injected a fluorochrome-labeled anti-CD45.1 antibody intravenously five minutes prior to sacrifice to exclude intravascular recipient CD45.1⁺ cells from the analysis. We identified 8 T cell populations (Supplemental Figures 5A, B). We evaluated Foxp3 cells within this dataset, which had 3 discrete sub-populations (Figure 3C, left; Supplemental Figure 6A). We found graft-resident (CD45.2⁺) regulatory T cells

exhibited a markedly distinct transcriptional profile compared to graft-infiltrating (CD45.1⁺) extravasated regulatory T cells 7 days after re-transplantation (Figure 3D). Graft-infiltrating (CD45.1⁺) extravasated regulatory T cells shifted their transcriptional profile at 21 compared to 7 days after re-transplantation. The transcriptional profile for day 21 graft-infiltrating (CD45.1⁺) extravasated regulatory T cells revealed downregulation of many genes expressed in these cells at day 7 after re-transplantation and began to resemble graft-resident (CD45.2⁺) regulatory T cells at 7 days after re-transplantation. Most notably, day 7 graft-resident (CD45.2⁺) and day 21 graft-infiltrating (CD45.1⁺) extravasated regulatory T cells had higher expression of *Areg* (gene encoding amphiregulin), *Ctla4* (gene encoding CTLA4), *Tnfrsf18* (gene encoding CD357/glucocorticoid-induced TNFR-related protein (GITR)), *Tnfaip3* (gene encoding A20) and *Hopx* compared to day 7 graft-infiltrating (CD45.1⁺) extravasated regulatory T cells (Supplemental Figures 6B, C).

Similar to our observations for regulatory T cells, the transcriptional profile of day 21 graft-infiltrating (CD45.1⁺) extravasated CD8⁺ and non-regulatory CD4⁺ T cells resembled the respective day 7 graft-resident (CD45.2⁺) to a greater degree than day 7 graft-infiltrating (CD45.1⁺) extravasated T cell populations (Supplemental Figure 7). Compared to day 7 graft-infiltrating (CD45.1⁺) CD8⁺ T cells, day 7 graft-resident (CD45.2⁺) and day 21 graft-infiltrating (CD45.1⁺) CD8⁺ T cells had higher expression levels of *Pdcd1* (gene encoding PD-1), *Ctla4*, *Lag3* (gene encoding lymphocyte-activation gene 3) and *Il2rb* (gene encoding the interleukin-2 receptor subunit beta), markers associated with exhaustion and/or immunoregulation (Supplemental Figure 7B) (18, 19). We also examined the single-cell TCR profiles of graft-resident (CD45.2), graft-infiltrating (CD45.1) and splenic (CD45.1) Foxp3⁺ cells 4 days after re-transplantation of tolerant Balb/c (CD45.2) lungs (previously transplanted into CSB-treated B6 (CD45.2) mice) into non-

immunosuppressed B6 (CD45.1) recipients. Compared to graft-resident (CD45.2) Foxp3⁺ cells, we observed a greater clonal diversity in graft-infiltrating (CD45.1) and splenic (CD45.1) Foxp3⁺ cells (Supplemental Figure 8). Finally, when compared to graft-infiltrating Foxp3⁺ cells, graft-resident Foxp3⁺ cells were shifted from a central (CD44^{hi}CD62L^{hi}) to an effector memory (CD44^{hi}CD62L^{low}) phenotype 7 days after re-transplantation (Figures 3E-I).

Depletion of recipient Foxp3⁺ cells results in loss of allograft tolerance with development of AMR and ACR

To understand the role of recipient-derived graft-infiltrating Foxp3⁺ cells, we used B6 Foxp3 diphtheria toxin receptor (DTR) mice as secondary recipients of previously tolerized Balb/c lung allografts (Figure 4A). Treatment of these mice with diphtheria toxin (DT) after re-transplantation allowed us to selectively deplete recipient Foxp3⁺ cells while preserving graft-resident Foxp3⁺ cells (Supplemental Figure 9). Control transplants where secondary B6 wildtype recipients were treated with DT were ventilated 7 days after re-transplantation (Figure 4B). Consistent with previous reports, these allografts exhibited intact airspaces with preservation of BALT on histological examination (Figure 4B). Additionally, immunostaining revealed CCSP expression in the airways (Figure 4B). Finally, we examined complement 4d (C4d) deposition, a marker of complement activation, and found no positive staining in these control re-transplanted lungs (Figure 4B). Altogether, these findings confirm our previous observations that lung allograft tolerance is maintained following re-transplantation into a non-immunosuppressed B6 recipient that is sufficient in Foxp3⁺ cells (7). Conversely, when we depleted recipient Foxp3⁺ cells, the re-transplanted lung was not ventilated (Figure 4C). We observed histological hallmarks of AMR, including neutrophilic capillaritis, flattening of the airway epithelium, obliterated alveolar spaces

filled with hyaline membrane deposition, loss of CCSP expression and endothelial C4d deposition (Figure 4C) (20). Compared to control re-transplants a higher proportion of graft-infiltrating recipient B cells in recipient Foxp3-depleted re-transplants expressed CD69 and Fas (Figures 4D, E) and more often underwent class-switch recombination as evidenced by lack of surface IgM and IgD expression (Figure 4F). Recipient Foxp3-depletion also resulted in higher serum levels of IgM donor-specific antibodies (DSAs) compared to control conditions (Figure 4G; Supplemental Figure 10). In addition, Foxp3-depletion resulted in concomitant ACR as evidenced by perivascular mononuclear infiltrates with endothelialitis (Figures 4C, H). Thirty days after re-transplantation of tolerant lung allografts, recipient Foxp3-depletion resulted in graft necrosis (Supplemental Figure 11). Collectively, these findings demonstrate that lung allografts lose their tolerant state and undergo changes consistent with AMR with concomitant ACR in the absence of continuous replenishment of Foxp3⁺ cells from the recipient.

Rejection after recipient Foxp3⁺ cell depletion is dependent on B cells

To further assess the role of B cells in recipient Foxp3-depletion mediated rejection, we transplanted Balb/c lungs into CSB-treated B6 CD11c-EYFP mice. At least 30 days later, these tolerized allografts were re-transplanted into non-immunosuppressed B6 Foxp3-GFP recipients. We adoptively transferred recipient-matched B6 9-[2-carboxy-4(or 5)-[[4-(chloromethyl)benzoyl]amino]phenyl]-3,6-bis(dimethylamino)-xanthylum (CMTMR)-labeled (red) B cells two days after re-transplantation and imaged the lung grafts intravitaly one day later. In areas of BALT characterized by CD11c⁺ cell aggregates, we observed prolonged interactions between recipient-derived Foxp3⁺ and B cells (Figure 5A; Supplemental Video 3). We next treated secondary non-immunosuppressed B6 recipients of tolerized Balb/c lung allografts with anti-

CD20 antibodies to deplete B cells concurrent with the depletion of recipient Foxp3⁺ cells (Supplemental Figure 12). In contrast to recipients that received isotype control antibodies, B cell depletion substantially reduced inflammatory changes characteristic of AMR and significantly reduced serum levels of IgM DSAs seven days after re-transplantation (Figures 5B, C). In addition, B cell depletion reduced the severity of ACR (Figure 5D). To gain additional mechanistic insight into the role of antibody production by recipient B cells in the rejection process in our model, we re-transplanted tolerant lung allografts into anti-CD25 antibody (PC61)-treated B6 wildtype or AID/ μ S knockout mice (AID/ μ S knockout mice have B cells that cannot secrete antibodies but can function as antigen presenting cells) (Supplemental Figure 13). B6 AID/ μ S knockout recipients did not form donor-specific IgM antibodies. Compared to PC61-treated B6 wildtype mice, allograft inflammatory changes and the severity of ACR were reduced after transplantation into AID/ μ S knockout recipients. Thus, lung graft rejection induced by recipient Foxp3⁺ cell depletion is dependent on B cell-mediated immune responses.

Lung allograft tolerance is maintained in the global absence of CD4⁺ T cells

Our previous work has shown that recipient B cells require T cell help to mediate rejection when graft-resident Foxp3⁺ cells are depleted (6). Therefore, we next set out to examine the effect of complete absence of recipient CD4⁺ cells on the maintenance of tolerance. For this purpose, we transplanted Balb/c lungs into CSB-treated B6 recipients and then, at least 30 days later, re-transplanted these tolerized grafts into B6 CD4-deficient secondary hosts. CD4-deficient mice lack conventional CD4⁺ T cells in addition to regulatory CD4⁺Foxp3⁺ cells. At both seven (Figures 6A-C) and 30 days (Supplemental Figure 14) after re-transplantation, lung allografts were ventilated, and the graft architecture remained intact with preservation of BALT. In the absence of recipient

CD4⁺ cells, serum levels of IgM DSAs did not differ significantly from control re-transplants with wildtype secondary recipients (Figure 6D).

IL-33 promotes the expansion and activation of lung allograft-resident Foxp3⁺ cells

IL-33 is cytokine that drives T_H2 immunity and activation of innate lymphoid cells (21, 22), but it has also been shown to be critical in maintaining homeostasis of tissue-resident regulatory T cells (23, 24). To study the effect of exogenous IL-33 administration in our model, we transplanted Balb/c lungs into CSB-treated B6 recipients. At least 30 days later, we administered recombinant IL-33 or phosphate-buffered saline (PBS) control intratracheally and examined the T cell composition in the lung allografts seven days later. We observed a significant expansion of the CD4⁺Foxp3⁺ T cell population in IL33-treated mice when compared to PBS controls (Figure 7A). While IL-33 injection did not alter the proportion of CD4⁺Foxp3⁺ cells that express CD25, it did increase the proportion of effector memory CD4⁺Foxp3⁺ cells (T_{EM}, CD44^{hi}CD62L^{lo}), decreased central memory CD4⁺Foxp3⁺ cells (T_{CM}, CD44^{hi}CD62L^{hi}) and resulted in a higher proportion of CD4⁺Foxp3⁺ cells expressing CD69 and PD-1 (Figures 7B-E). IL-33 treatment did not have a significant effect on the memory phenotype of graft-resident CD8⁺ T cells (Supplemental Figure 15). We next wanted to determine whether intratracheal IL-33 administration expands CD4⁺Foxp3⁺ cells in the allograft by directly acting on Foxp3⁺ cells. To this end, we transplanted Balb/c lungs into CSB-treated B6 Foxp3-YFP-Cre *St2^{fl/fl}* or B6 Foxp3-YFP-Cre controls. There was significantly less expansion of intragraft Foxp3⁺ cells following intratracheal treatment with IL-33 when Foxp3⁺ cells did not express ST2 (Supplemental Figure 16). Thus, having observed that local administration of IL-33 induces the expansion and activation of graft-resident CD4⁺Foxp3⁺ cells, we next set out to examine whether this treatment prevents rejection when

graft-resident Foxp3⁺ cells are not replenished. To this end, we transplanted Balb/c lungs into CSB-treated B6 recipients. At least 30 days later these tolerized allografts were re-transplanted into non-immunosuppressed DT-treated B6 Foxp3-DTR mice. We administered recombinant IL-33 or PBS into their airways and examined the mice seven days later. We found that intratracheal IL-33 therapy reduced the inflammatory changes characteristic of AMR and severity of ACR (Figure 7F, G). Compared to control PBS-treated re-transplants, IL-33 administration resulted in significant reductions of serum IgM DSAs levels (Figure 7H).

Discussion

Mechanisms of tolerance after solid organ transplantation differ by organ. Our observations extend previous findings from our laboratory and others that immunoregulatory pathways are established locally in the lung graft (6, 7, 17, 25). In this study, we show that the preservation of graft-resident Foxp3⁺ cells is critical for the maintenance of lung allograft tolerance. Using a mouse lung re-transplant model, we demonstrate that the pool of tissue-resident Foxp3⁺ cells is maintained through continuous replenishment with Foxp3⁺ cells that are recruited from the periphery to the graft. Waldmann's group described the concept of self-sustaining "infectious tolerance" in skin transplant models, where Foxp3⁺ cells can induce the generation of new Foxp3⁺ cells from naïve T cells (26, 27). By contrast, our study shows that Foxp3⁺ cells that are recruited to tolerant lung allografts are not derived from peripheral conversion of non-regulatory T cells. We demonstrate that graft-resident Foxp3⁺ cells are largely of thymic origin and have distinct features that have been described for regulatory T cells residing in various non-lymphoid tissues (28-30). Finally, our experiments suggest that lung graft-resident Foxp3⁺ cells can be potentially targeted with inhaled immunomodulatory agents.

Our group has previously reported that tolerance induction after lung transplantation depends on production of IFN- γ by central memory CD8⁺ T cells, which drives the production of nitric oxide (3). We showed that at 7 days after transplantation, the proportion of intra-graft CD4⁺ T cells expressing Foxp3 was lower when recipients lacked CD8⁺ T cells. While future studies will need to explore this association mechanistically, reports exist that IFN- γ and nitric oxide can promote the expansion of regulatory CD4⁺Foxp3⁺ T cells (31, 32). Here, we show that graft-resident CD8⁺ T cells in long-term tolerant lung allografts express markers that are characteristic of exhaustion and/or immunoregulation. This observation is consistent with a recent report

showing that CD8⁺ T lymphocytes that infiltrate spontaneously accepting mouse kidney allografts are reprogrammed to exhausted/regulatory-like cells (19).

AMR has been increasingly recognized as a cause for severe graft dysfunction after lung transplantation and also as a risk factor for the development of chronic lung allograft dysfunction (2). To this end, we and others have previously reported that humoral alloimmune responses are critical drivers of chronic fibrotic remodeling after lung transplantation (33, 34). We have shown that depletion of graft-resident Foxp3⁺ cells results in the local activation of B cells and AMR (6). The use of a mouse lung re-transplant model enabled us to selectively deplete graft-infiltrating Foxp3⁺ cells while preserving graft-resident Foxp3⁺ cells (35). We demonstrate that in the absence of continuous recruitment of Foxp3⁺ cells to the transplanted lung, graft-resident Foxp3⁺ cells alone are not sufficient to prevent rejection. Histologically, rejected allografts have features characteristic of AMR including a pattern of acute lung injury with hyaline membrane formation, neutrophilic capillaritis, loss of CCSP expression and complement deposition along with ACR (20). A case series from our center reported ACR in 29% of human lung transplant recipients who were diagnosed with C4d-positive AMR (36). However, given potential sampling errors associated with transbronchial biopsies, the incidence of concomitant AMR and ACR in humans may be higher. We show that graft-infiltrating Foxp3⁺ cells interact with newly recruited B cells, and B cell depletion reduces the severity of AMR and ACR. These observations raise the possibility that – in addition to mediating AMR through production of alloantibodies – B cells may exacerbate ACR through their function as antigen presenting cells. While we and others have previously used anti-CD25 antibodies to deplete regulatory T cells we recognize that this approach has some limitations, including an incomplete depletion due to the presence of Foxp3⁺CD25^{low} cells and an inability to target donor vs. recipient regulatory T cells (7, 37, 38). Nevertheless, the reduction in

severity of ACR after treatment of AID/ μ S-deficient recipients with PC61 raises the possibility that antibody production by B cells, directly or indirectly, may contribute to the activation of T cells (39, 40).

Unlike the case with selective depletion of recipient Foxp3⁺ cells, global absence of recipient CD4⁺ cells did not trigger rejection. We have previously reported that the generation of DSAs is inhibited, and graft rejection is attenuated after depletion of graft-resident Foxp3⁺ cells when recipients lack T cells or when CXCL13, the ligand for CXCR5, is neutralized (6). These findings support the notion that B cell activation in the context of Foxp3⁺ cell depletion-mediated graft rejection requires CD4⁺ T cell help, which is presumably provided by graft-infiltrating CD4⁺CXCR5⁺ T follicular helper cells.

Phenotypic and transcriptional differences between graft-resident and newly recruited Foxp3⁺ cells suggest that their functions are imprinted within the transplanted lung. This notion is further supported by their clonal expansion in the graft, a finding that mirrors observations for tissue-resident regulatory T cells in other locations (29, 30). Previous work has proposed a two-step model for the acquisition of the phenotype of regulatory T cells that reside in visceral adipose tissue, where an initial priming step in the spleen is followed by further education in the non-lymphoid tissue (41). In previous work we have shown that Foxp3⁺ cells leave the BALT within tolerant lung allografts via lymphatics and suppress alloimmune responses in the periphery to donor-matched but not third-party grafts (17). Previous studies have shown that transplantation of vascularized donor thymic tissue along with an allograft results in downregulation of alloimmune responses (42). While several mechanisms have been proposed, the beneficial effects of thymic grafting on allograft survival could – at least in part - be due to migration of regulatory T cells from the thymic graft to the periphery (43). Our observations suggest that the suppressive capacity

of Foxp3⁺ cells, both locally and systemically, is dependent on alloantigen recognition and clonal expansion in the allograft, which likely occurs within the BALT. The requirement for continuous replenishment of the allograft tissue-resident Foxp3⁺ cell population raises several not mutually exclusive possibilities. Tissue-resident Foxp3⁺ cells could have a limited lifespan, which could be a function of insufficient levels of cytokines within the BALT that promote their survival. Foxp3⁺ cells could become unstable within the graft environment and lose their suppressive function. Finally, Foxp3⁺ cells could continuously egress from the graft and migrate to the periphery; however, this is not likely to be a dominant mechanism in our experimental system as lymphatic drainage from the allograft is not reestablished until several weeks after transplantation (17, 44).

In addition to their clonal expansion, important similarities exist between Foxp3⁺ cells that reside within tolerant lung allografts and regulatory T cells that have been described and characterized in other non-lymphoid tissues. For example, regulatory T cells within visceral adipose tissue express high levels of Helios and Neuropilin-1 and Foxp3⁻ cells do not convert into Foxp3⁺ cells indicating that these cells are likely of thymic origin (28). Similarly, regulatory T cells that accumulate in injured skeletal muscles express Helios and Neuropilin-1 (30). Moreover, the transcriptome of muscle-resident regulatory T cells is distinct from that in regulatory T cells that reside in secondary lymphoid organs. Of note, similar to our observations in tolerant lung allografts, regulatory T cells that reside in skeletal muscle and visceral adipose tissue express ST2, the receptor for IL-33 (28, 30).

IL-33 is a pro-inflammatory IL-1 family cytokine expressed at epithelial tissue barriers and a nuclear alarmin that alerts innate immune cells and T_H2 lymphocytes to injury or infection (45). This cytokine is also known to promote type 1 immune responses against tumors (46). However, IL-33 plays important roles in downregulating deleterious immune responses (47). For

example, our group has recently reported that ischemia reperfusion injury after lung transplantation increases the expression of IL-33 in airway epithelial cells (48). IL-33 drives IL-5 production by innate lymphoid cells (ILC) type 2, which facilitates the recruitment of eosinophils and tolerance induction. We show that local administration of IL-33 expands and activates lung allograft-resident Foxp3⁺ cells. This observation extends findings from several studies that have demonstrated the capacity of IL-33 to expand tissue-resident regulatory T cells in various sites (23, 24, 28, 49-51). IL-33 can mediate its effect by signaling through several pulmonary cell populations. For example, a recent study showed that IL-33-ST2 signaling in macrophages promotes club cell repair after naphthalene-induced injury (52). We show that IL-33-mediated expansion of Foxp3⁺ cells in lung allografts is – at least in part – dependent on *St2* expression by Foxp3⁺ cells. We also demonstrate that intra-airway IL-33 administration reduces the severity of AMR and ACR at 7 days after re-transplantation when recruitment of Foxp3⁺ cells to the allograft is prevented. Our observations extend previous findings that IL-33 treatment prolongs the survival of murine cardiac and skin allografts, an effect that is dependent on regulatory T cells (53, 54).

IL-33 has also been reported to potentially contribute to various lung diseases, including pulmonary fibrosis, asthma and chronic obstructive pulmonary disease (55-57). While we show beneficial effects at 7 days after re-transplantation, additional long-term studies are required to assess the efficacy and safety of local IL-33 administration in lung transplant recipients. Nevertheless, the critical role that tissue-resident Foxp3⁺ cells play in maintaining tolerance after lung transplantation provides a compelling rationale for exploring local therapies, especially since their proximity to airways due to their accumulation in the BALT renders them accessible to inhaled agents. Local immunosuppressive therapies are appealing for lung transplant patients as they may decrease the harmful side effects of systemic therapy (58). We have recently reported

that cyclosporine-based immunosuppression triggers rejection of tolerant lung allografts (59). Our flow cytometry and gene expression data indicate that a portion of tissue-resident Foxp3⁺ cells in tolerant lung allografts expresses CD25, the alpha subunit of the IL-2 receptor. As cyclosporine is known to suppress IL-2, studies are warranted that examine the effect of local IL-2 administration on lung transplant tolerance. A recent study showed that systemic treatment of mouse lung transplant recipients with IL-2/anti-IL-2 antibody complexes prior to engraftment facilitated long term survival which was dependent on accumulation of Foxp3⁺ cells in the allograft (25).

The continuous replenishment of Foxp3⁺ cells from peripheral sites points to therapeutic strategies in addition to the local administration of cytokines that promote their survival and activation. To this end, an important area for future investigation is to define chemotactic gradients that guide recipient Foxp3⁺ to the BALT within tolerant lung allografts. Future studies could focus on the role of CXCL12 as we observed that, compared to graft-resident Foxp3⁺ cells, recently recruited Foxp3⁺ cells express higher levels of CXCR4. Interestingly, tolerance after vascularized composite allotransplantation is dependent on the presence of CXCR4-expressing Foxp3⁺ cells in the bone marrow, which may at least in part be due to guiding the accumulation of regulatory T cells in specific niches (60). Requirements for specific chemotaxins may differ between transplanted tissues. For example, tolerance after rat kidney transplantation is associated with production of CCL5 by myeloid-derived suppressor cells, which mediates the recruitment of regulatory T cells to the graft (61). CCL22 overexpression in pancreatic islet transplants attracts regulatory T cells and protects the grafts (62).

One noteworthy gene that is highly expressed by tissue-resident Foxp3⁺ cells in tolerant lung allografts is amphiregulin, a growth factor that signals through EGFR. Amphiregulin plays an important role in tissue homeostasis and repair after injury. In a model of pulmonary

hypertension, amphiregulin produced by endothelial cells is thought to signal in an autocrine fashion to promote endothelial cell survival and proliferation (63). Notably, in a mouse model of respiratory viral infection, regulatory T cells play a critical role in tissue repair via their production of amphiregulin that is distinct from their immunosuppressive role (64). In skeletal muscle, amphiregulin signals to muscle satellite cells and myoblasts for muscle regeneration after injury. Ablation of Foxp3⁺ cells compromises muscle repair, whereas exogenous amphiregulin administration to Foxp3⁺ cell-ablated mice was associated with upregulation of muscle repair genes and enhanced myogenic differentiation of satellite cells (30). While some studies have shown that amphiregulin enhances the suppressive capacity of regulatory T cells, EGFR expression was largely restricted to stromal cells in our lung grafts (65, 66). Thus, the severe inflammation that we observe when recipient Foxp3⁺ cells lack *Areg* suggests that Foxp3-derived amphiregulin maintains a homeostatic state by directly acting on intragraft stromal cell populations.

In conclusion, we characterize a graft-resident Foxp3⁺ cell population following lung transplantation that is critical in maintaining tolerance. These cells accumulate within BALT where they acquire unique features and need to be continually replenished by recipient-derived Foxp3⁺ cells. Our findings highlight the importance of preserving this cell population in lung allografts, which may be achieved through local therapy.

Methods

Sex as a biological variable

Our study examined male and female animals, and similar findings are reported for both sexes.

Mice and Reagents

Mouse strains including C57BL/6J (B6 CD45.2), B6.SJL-PtprcaPepcb/BoyJ (B6 CD45.1), Balb/cJ, B6.Cg-Tg(Itgax-Venus)1Mnz/J (B6 CD11c-EYFP), B6 Foxp3tm9(EGFP/cre/ERT2)Ayr/J (B6 Foxp3-internal ribosome entry sites (IRES)-GFP) (referred to as B6 Foxp3-GFP), B6-Foxp3tm1Flv/J (B6 Foxp3-IRES-RFP) (referred to as B6 Foxp3-RFP), B6-Tg(Foxp3-HBEGF/EGFP)23.2Spar/Mmjax (B6 Foxp3-DTR), and B6.129S2-Cd4tm1Mak/J (B6 CD4KO) were purchased from The Jackson Laboratory. B6 CD11c-EYFP/Foxp3-IRES-GFP mice were generated by crossing B6 CD11c-EYFP mice with B6 Foxp3-IRES-GFP mice. B6 Foxp3-YFP-Cre *Areg*^{fl/fl}, B6 Foxp3-YFP-Cre *St2*^{fl/fl} and B6 Foxp3-YFP-Cre littermate controls were provided by H.R. Turnquist (The University of Pittsburgh, Pittsburgh, PA). B6 AID/ μ S (activation-induced cytidine deaminase / secretory μ -chain)-deficient mice were originally provided by G. Chalassani (The University of Pittsburgh, Pittsburgh, PA) after obtaining permission from F. Lund (University of Alabama, Birmingham, AL) and maintained in our colony. Six- to ten-week-old sex-matched mice were used for transplant procedures. Following primary lung transplant, CSB was administered to the recipient mouse with anti-CD40 ligand (250 μ g intraperitoneally (i.p.)) and CTLA4-Ig (200 μ g i.p.) on post-operative days 0 and 2, respectively (BioXCell). DT (Sigma-Aldrich) was administered into re-transplant recipients (250 μ g i.p. on post-operative days 0, 1, and 4 and then weekly as indicated). For select experiments, 250 μ g of anti-CD20 neutralizing antibody (BioXCell) was administered intravenously (i.v.) to the recipient

one day prior to re-transplantation, and then i.p. on post-operative days 0, 1, and 4 following re-transplantation, with IgG2c isotype serving as control (BioXCell). For some experiments, PC61 (BioXCell) was administered i.p. to re-transplant recipients on days 0 (500µg), 1 and 3 (250 µg each). Three doses of recombinant mouse IL-33 (50 µg/50 µl) (Biolegend) were administered into the airways of primary recipients (≥ 30 days after transplantation as well as 1 and 4 days later) and re-transplant recipients (days 0, 1 and 4), with PBS serving as control.

Surgical procedure

Orthotopic left lung transplants and re-transplants were performed, as previously described (35, 67).

Flow cytometry

Lung digestion and preparation of single cell suspension were performed as previously described (3). Flow cytometry antibodies used were as follows: CD4 (clone GK1.5), CD44 (IM7), and CD69 (H1.2F3) (BioLegend); Foxp3 (FJK-16s), CD62L (MEL-14), Helios (22F6), PD-1 (J43), IgM (II/41), CD45.1 (A20), CD19 (1D3) (Invitrogen); CD25 (PC61), CD45R (RA3-6B2), CD95 (Jo2), IgD (11-26c.2a), CD8a (53-6.7), CD45.2 (104), CD90.2 (53-2.1), CD45 (30-F11) (BD Biosciences) and CD304 (Neuropilin-1) (3DS304M) (eBioscience). Serum IgM DSA titers were determined with polyclonal fluorochrome-conjugated goat anti-mouse IgM (μ chain-specific), as previously described (Jackson ImmunoResearch)(6). Differences between groups for serum DSA levels were determined at serum dilutions of 1:8. Cells were analyzed on a FACScan (BD) and Attune NxT Acoustic Focusing Cytometer (Thermo Fisher Scientific). Acquired flow cytometric

data were analyzed with FlowJo v10.9 (FlowJo, BD). Live gates defined by forward- and sidescatter characteristics were used for analyses.

Cell isolation and adoptive transfer

For B cell adoptive transfer experiments, B cells were isolated from spleens of naïve B6 mice using a B cell isolation kit (Miltenyi Biotec). Cells were stained with CMTMR (Thermo Fisher) and 2×10^6 B cells were injected i.v. into recipient mice. For Foxp3-GFP⁻ cell adoptive transfer experiments, live CD45⁺CD90⁺CD4⁺GFP⁻ cells were purified by fluorescence-activated cell sorting from spleen and lymph nodes of B6 Foxp3-IRES-GFP (CD45.1) mice using a MoFlo sorter (BD) and 5×10^6 cells were injected into the recipient mouse via the right internal jugular vein.

Intravital two-photon microscopy

Lung grafts were imaged by intravital two-photon microscopy, as previously described (11). Twenty μL of 655-nm nontargeted quantum-dots (q-dots, Life Technologies) in 50 μL of PBS or 8 μL of dextran-rhodamine B (30,000MV, Invitrogen), suspended in 150 μL of PBS were injected intravenously to label blood vessels. CMTMR-labeled B cells were isolated and injected 2 days after re-transplantation into lung recipients and 24 hours prior to imaging. Grafts were stabilized within the left chest and imaged with a custom two-photon microscope using SlideBook v6 (Intelligent Imaging Innovations, Inc. CO). Sequential z-sections (2.0 μm each) were acquired, yielding an imaging volume of $330 \times 330 \times 40 \mu\text{m}^3$. Videos and images were acquired and processed with Imaris 9.7.2 (Bitplane).

Histology

Transplanted and re-transplanted lungs were fixed in formaldehyde, embedded in paraffin, and sectioned into 5 µm slices. Lung sections were stained with hematoxylin and eosin and assessed for AMR and graded for acute cellular rejection (International Society for Heart and Lung Transplantation (ISHLT) A grades) by a blinded pathologist (J.H.R.).

Immunofluorescence and immunohistochemistry

Formalin-fixed, paraffin-embedded 5 µm mouse lung sections were deparaffinized and rehydrated. Antigen retrieval was performed in a pH 6.0 citrate-based buffer (Vector Labs) at 100°C for 20 minutes, followed by three 5-minute washes in PBS with 1% Tween (PBS-T). For immunofluorescent staining, non-specific binding was blocked with 10% normal goat serum (Invitrogen). Slides were co-stained with rabbit anti-mouse polyclonal CCSP (1:250, Seven Hills Bioreagent, catalog # WRAB-3950) and incubated overnight at 4°C. Slides were washed with PBS-T and then incubated with goat anti-rabbit AlexaFluor (AF)-488 (ThermoFisher, catalog # A-11008) for 45 minutes. After three PBS-T washes, the slides were counterstained with nuclear stain Hoechst 33342 (1:1000, Invitrogen, catalog # H3570) for 15 minutes. Slides were coverslipped with aqueous mounting medium (Invitrogen). For immunohistochemical staining, endogenous hydrogen peroxidase and alkaline phosphatase were quenched with BLOXALL endogenous blocking solution (Vector Labs), non-specific protein binding was blocked with 10% goat serum (Vector Labs), non-specific avidin/biotin binding was blocked with Avidin/Biotin block (Vector Labs). Slides were stained with rabbit anti-mouse polyclonal C4d (1:100, Hycult Biotech, catalog # HP8033) overnight at 4°C, washed, and then stained with biotinylated goat-anti rabbit IgG (1:200, Vector Labs, catalog # BA-1000-1.5) for 30 minutes. Antibody binding was

amplified with the Vectastain ABC Kit (Vector Labs) and visualized with peroxidase substrate 3,3-diaminobenzidine (Vector Labs). Slides were counterstained with hematoxylin (Leica Biosystems) and coverslipped with non-aqueous mounting medium (Thermo Fisher Scientific). Human slides were stained with 1:200 rat anti-human foxp3 (clone PCH101, eBioscience) at room temperature for 2 hours, then amplified and visualized with VECTASTAIN ABC Kit, Peroxidase (Rat IgG) (Vector Labs). The slides were incubated with 1:200 polyclonal rabbit amphiregulin (catalog # bs-3847R, Bioss) overnight and then amplified and visualized with Vectastain ABC Kit, Alkaline Phosphatase (Rabbit IgG) (Vector Labs). All images were acquired using an Olympus BX61 microscope with a digital camera and CellSens Dimension software (Olympus, Version 1.18).

Single cell suspension preparation for single-cell RNA sequencing

For comparison of Foxp3⁺ cells in tolerant lung allografts and spleen, transplanted left lungs and recipient spleens were collected at least 30 days after transplantation of Balb/c lungs into CSB-treated B6 Foxp3-GFP recipients. Lung tissue was digested, and single-cell suspensions were prepared as previously described (68). Cells were stained using antibodies specific for CD45, CD90.2, CD4, CD8a and 4',6-diamidino-2-phenylindole (DAPI) (BD Biosciences) and were sorted by flow cytometry for CD45⁺CD90.2⁺CD4⁺CD8a⁻GFP⁺ cells into a 250 μ L cell resuspension buffer (0.04% bovine serum albumin (BSA) in PBS). Collected cells were centrifuged (300 relative centrifugal force for 5 minutes at 4 °C) and resuspended in collection buffer to a target concentration of 1,000 cells/ μ L. Cells were counted on a hemocytometer before proceeding. For comparison of graft-resident versus graft-infiltrating T cells, lungs from Balb/c donors transplanted into CSB-treated B6 (CD45.2) primary recipients, and then re-transplanted

into B6 (CD45.1) secondary recipients at least 30 days later, were harvested at seven or 21 days after re-transplantation. A fluorochrome-labeled anti-CD45.1 antibody was injected intravenously (CD45.1-i.v.) into recipient mice 5 minutes prior to sacrifice to allow for exclusion of intravascular cells. Cells were stained using antibodies specific for CD90.2, Lin (CD19, NK1.1, CD11b, Ly6G), CD45.2, CD45.1 and DAPI (BD Biosciences) and were sorted by flow cytometry for DAPI⁻ CD90.2⁺Lin⁻CD45.2⁺CD45.1⁻ or DAPI⁻CD90.2⁺Lin⁻CD45.2⁻CD45.1⁺CD45.1-i.v.⁻ cells. For analysis of TCR clonotypes in regulatory T-cells in re-transplant recipients lungs from Balb/c donors transplanted into CSB-treated B6 (CD45.2) primary recipients, and then re-transplanted into B6 (CD45.1) secondary recipients at least 30 days later, were harvested along with recipient spleens 4 days after re-transplantation. Cells were stained using antibodies specific for CD90.2, Lin (CD19 (clone 1D3, eBioscience), NK1.1 (clone PK136, BioLegend), CD11b (clone M1/70, Invitrogen), Ly6G (clone 1A8, BD Biosciences)), CD4, CD8a, CD45.2, CD45.1 and DAPI (BD Biosciences) and were sorted by flow cytometry for DAPI⁻ Lin⁻ CD45.2⁺CD45.1⁻ CD90.2⁺CD4⁺CD8a⁻ or DAPI⁻ Lin⁻CD45.2⁻CD45.1⁺CD90.2⁺CD4⁺CD8a⁻ cells. Single cell suspensions were prepared, as described above.

Library preparation for single-cell RNA sequencing and TCR profiling

Single-cell suspensions were submitted to the Genome Technology Access Center core facility (Washington University) for single-cell genome-scale metabolic models (GEM) construction and complementary deoxyribonucleic acid (cDNA) synthesis and library construction. For the sorted Foxp3⁺ cells, cells were labeled using TotalSeq anti-mouse hashtag antibodies (Biolegend) prior to sample submission. For the primary transplants, two sets of hashtagged samples were submitted for genome sequencing and TCR profiling. Samples were processed using the Chromium Single

Cell 3' Library & Gel Bead Kit (10X Genomics, v3) and Chromium Single Cell V(D)J Reagent Kits (10x Genomics) following manufacturer's protocols. The libraries were sequenced on NovaSeq S4 (Illumina) targeting 50,000 reads per cell and 500 million read pairs per library. Cells were aligned to the mouse mm10-2020-A transcriptome using Cell Ranger (10x Genomics, v6.1.1) to generate feature-barcoded count matrices. For TCR analysis of re-transplants we used Chromium Next GEM Single Cell 5' Kit v2 with paired T cell receptor sequencing.

Analysis pipeline for single-cell RNA sequencing and TCR profiling

Analysis was performed using the R Seurat v4.0.0 package. The following quality control steps were performed to filter the count matrices: 1) Cells expressing fewer than 500 genes were removed; 2) cells expressing over 10,000 genes were discarded as these could be potential multiplet events where more than a single cell was encapsulated within the same barcoded GEM; 3) cells with >5% mitochondrial content were filtered out as these were deemed to be of low quality (69). Following quality control, normalization and variance-stabilization of raw counts was performed using SCTransform, and cell cycle scores were computed and regressed out in combination with percentage mitochondrial reads (70). The normalized R object was then used for subsequent clustering and differential expression testing and integration with harmony was performed (71). Briefly, clusters were annotated into major cell populations, each major cell type was subsetted, and re-normalized, PCA, UMAP embedding, clustering, and differential expression analysis performed. Clusters which resembled low quality cells or doublets were removed from subsequent analysis. We used the FindAllMarkers function in Seurat to perform differential expression testing and annotated clusters into distinct cell types based on canonical gene markers. For downstream TCR analysis in primary transplants, TCRs with only one pair of productive

rearrangements for TCR α and TCR β chains were selected. Clonotypes in each sample were defined based on identical CDR3 nucleotide sequences together with identical V and J genes in both TCR α and TCR β chains. Gini coefficients in each sample were calculated using Gini function from the DescTools package v0.99.50. Shared clonotypes were defined as clonotypes coming from different tissues within same mouse and containing identical CDR3 nucleotide sequences together with identical V and J genes. Visualization was performed with ggalluvial package v0.12.5. For analysis of TCR clonotypes in CD4⁺Foxp3⁺ regulatory T-cells in re-transplant recipients, the scRepertoire v 2.2.1 packaged was used in R. Briefly, filter contig outputs from the 10x Genomics CellRanger pipeline were used to assign clonotype data based on TCR α and TCR β chains. The clonalCompare function was used to visualize relative clonotypes across conditions. Clonal diversity was calculated using the Gini Simpson index with 20 bootstraps.

Sample preparation for single-nuclear RNA sequencing

Lung grafts from two mice per experimental group were harvested, embedded in optimal temperature control (OCT) compound, and flash frozen in liquid nitrogen. OCT embedded frozen tissue samples were processed for nuclei extraction by the Tissue Procurement Core at Washington University. Briefly, tissue from each sample was processed using the gentleMACS Octo Dissociator and cell lysis performed using Nuclei Extraction Buffer Protocol (Miltenyi Biotec). Nuclei suspensions from two mice per group were pooled, counted and resuspended at 1500 nuclei/ μ L in 1x phosphate buffered saline with 1% bovine serum albumin and 0.2 U/ μ L RNase inhibitor. Pooled nuclei suspensions were encapsulated with barcoded oligo-dT containing gel beads with the Chromium Single-Cell 3' Library & Gel Bead Kit (10X Genomics, v3) at the

Genome Technology Access Center at Washington University. Libraries were sequenced on the NovaSeq S4 (Illumina), with a target of 50,000 reads per cell and 500 million read pairs per library.

Statistics

Data were analyzed using Prism (GraphPad Software, Version 10.0.3) and presented graphically as mean \pm standard error of the mean. Groups were compared with the two-tailed unpaired Student's *t* test. A p-value of <0.05 was considered significant.

Study approval

Animal experiments were approved by the Institutional Animal Studies Committee at Washington University. Animals received humane care in compliance with the *Guide for the Care and Use of Laboratory Animals* (National Academies Press, 2011) and with the Principles of Laboratory Animal Care formulated by the National Society for Medical Research. Human protocols were approved by the Institutional Review Board at Washington University School of Medicine (no. 201811073).

Data availability

RNA-seq data generated in this study have been deposited in the NCBI's Gene Expression Omnibus (GEO) database under accession codes GSE251965 and GSE251931. The code has been uploaded to https://github.com/jamrute/2023_Kreisel_Foxp3_Transplant. Values for data presented in figures are provided in the Supporting Data Values file.

Author Contributions

WL, YT, YZB, YY, HMS, JMA, AIB, ZL, MT and JMG conducted experiments. WL, YT, YZB, AB, RGN, RRH, HRT, MNA, AA, PTS, KJL, ASK, AEG and DK contributed to study design and all authors reviewed and revised the manuscript. WL, YT, YZB, HMS, JMA, **AIB, ZL**, JMG, JHR, MNA and MT analyzed and interpreted the data. WL, YT, YZB, HMS and DK wrote the manuscript. DK designed and supervised the study. The order of the shared first authors (WL, YT, YZB) was determined based on relative contributions to study design, experimental work and preparation of manuscript draft and figures.

Acknowledgements

YZB is supported by the National Institutes of Health (NIH) grant T32HL007317. AEG is supported by NIH grants R01HL167277, R01HL094601, R01HL157407, P01AI116501, P41EB025815. DK is supported by NIH grants 1P01AI116501, R01HL151078, U01163086-01, Veterans Administration Merit Review grant 1I01BX002730, The Cystic Fibrosis Foundation and The Foundation for Barnes-Jewish Hospital. We thank the In Vivo Imaging Core at Washington University for assistance with imaging experiments. The graphical abstract was created in BioRender (<https://BioRender.com/n52h515>). The graphical abstract was created in BioRender (<https://BioRender.com/n52h515>) (Subscription Type: Postdoc Plan – Academic; Agreement Number AO27YI7KES).

References

1. Balsara KR, Krupnick AS, Bell JM, Khiabani A, Scavuzzo M, Hachem R, et al. A single-center experience of 1500 lung transplant patients. *J Thorac Cardiovasc Surg.* 2018;156(2):894-905 e3.
2. Witt CA, Puri V, Gelman AE, Krupnick AS, and Kreisel D. Lung transplant immunosuppression - time for a new approach? *Expert Rev Clin Immunol.* 2014;10(11):1419-21.
3. Krupnick AS, Lin X, Li W, Higashikubo R, Zinselmeyer BH, Hartzler H, et al. Central memory CD8⁺ T lymphocytes mediate lung allograft acceptance. *J Clin Invest.* 2014;124(3):1130-43.
4. Onyema OO, Guo Y, Wang Q, Stoler MH, Lau C, Li K, et al. Eosinophils promote inducible NOS-mediated lung allograft acceptance. *JCI Insight.* 2017;2(24).
5. Onyema OO, Guo Y, Mahgoub B, Wang Q, Manafi A, Mei Z, et al. Eosinophils downregulate lung alloimmunity by decreasing TCR signal transduction. *JCI Insight.* 2019;4(11).
6. Li W, Gauthier JM, Higashikubo R, Hsiao HM, Tanaka S, Vuong L, et al. Bronchus-associated lymphoid tissue-resident Foxp3⁺ T lymphocytes prevent antibody-mediated lung rejection. *J Clin Invest.* 2019;129(2):556-68.
7. Li W, Bribriescio AC, Nava RG, Brescia AA, Ibricevic A, Spahn JH, et al. Lung transplant acceptance is facilitated by early events in the graft and is associated with lymphoid neogenesis. *Mucosal Immunol.* 2012;5(5):544-54.
8. Zhao J, Jung S, Li X, Li L, Kasinath V, Zhang H, et al. Delivery of costimulatory blockade to lymph nodes promotes transplant acceptance in mice. *J Clin Invest.* 2022;132(24).
9. Zhang N, Schroppel B, Lal G, Jakubzick C, Mao X, Chen D, et al. Regulatory T cells sequentially migrate from inflamed tissues to draining lymph nodes to suppress the alloimmune response. *Immunity.* 2009;30(3):458-69.
10. Lindenberg M, Solmaz G, Puttur F, and Sparwasser T. Mouse cytomegalovirus infection overrules T regulatory cell suppression on natural killer cells. *Viral J.* 2014;11:145.
11. Kreisel D, Nava RG, Li W, Zinselmeyer BH, Wang B, Lai J, et al. In vivo two-photon imaging reveals monocyte-dependent neutrophil extravasation during pulmonary inflammation. *Proc Natl Acad Sci U S A.* 2010;107(42):18073-8.
12. GeurtsvanKessel CH, Willart MA, Bergen IM, van Rijt LS, Muskens F, Elewaut D, et al. Dendritic cells are crucial for maintenance of tertiary lymphoid structures in the lung of influenza virus-infected mice. *J Exp Med.* 2009;206(11):2339-49.
13. Halle S, Dujardin HC, Bakocevic N, Fleige H, Danzer H, Willenzon S, et al. Induced bronchus-associated lymphoid tissue serves as a general priming site for T cells and is maintained by dendritic cells. *J Exp Med.* 2009;206(12):2593-601.
14. Thornton AM, Korty PE, Tran DQ, Wohlfert EA, Murray PE, Belkaid Y, et al. Expression of Helios, an Ikaros transcription factor family member, differentiates thymic-derived from peripherally induced Foxp3⁺ T regulatory cells. *J Immunol.* 2010;184(7):3433-41.
15. Weiss JM, Bilate AM, Gobert M, Ding Y, Curotto de Lafaille MA, Parkhurst CN, et al. Neuropilin 1 is expressed on thymus-derived natural regulatory T cells, but not mucosa-generated induced Foxp3⁺ T reg cells. *J Exp Med.* 2012;209(10):1723-42, S1.

16. Singh K, Hjort M, Thorvaldson L, and Sandler S. Concomitant analysis of Helios and Neuropilin-1 as a marker to detect thymic derived regulatory T cells in naive mice. *Sci Rep.* 2015;5:7767.
17. Li W, Gauthier JM, Tong AY, Terada Y, Higashikubo R, Frye CC, et al. Lymphatic drainage from bronchus-associated lymphoid tissue in tolerant lung allografts promotes peripheral tolerance. *J Clin Invest.* 2020;130(12):6718-27.
18. Dai Z, Zhang S, Xie Q, Wu S, Su J, Li S, et al. Natural CD8+CD122+ T cells are more potent in suppression of allograft rejection than CD4+CD25+ regulatory T cells. *Am J Transplant.* 2014;14(1):39-48.
19. Yokose T, Szuter ES, Rosales I, Guinn MT, Liss AS, Baba T, et al. Dysfunction of infiltrating cytotoxic CD8+ T cells within the graft promotes murine kidney allotransplant tolerance. *J Clin Invest.* 2024;134(16).
20. Roux A, Levine DJ, Zeevi A, Hachem R, Halloran K, Halloran PF, et al. Banff Lung Report: Current knowledge and future research perspectives for diagnosis and treatment of pulmonary antibody-mediated rejection (AMR). *Am J Transplant.* 2019;19(1):21-31.
21. Buzzelli JN, Chaliner HV, Pavlic DI, Sutton P, Menheniott TR, Giraud AS, et al. IL33 Is a Stomach Alarmin That Initiates a Skewed Th2 Response to Injury and Infection. *Cell Mol Gastroenterol Hepatol.* 2015;1(2):203-21 e3.
22. McSorley HJ, Blair NF, Smith KA, McKenzie AN, and Maizels RM. Blockade of IL-33 release and suppression of type 2 innate lymphoid cell responses by helminth secreted products in airway allergy. *Mucosal Immunol.* 2014;7(5):1068-78.
23. Han JM, Wu D, Denroche HC, Yao Y, Verchere CB, and Levings MK. IL-33 Reverses an Obesity-Induced Deficit in Visceral Adipose Tissue ST2+ T Regulatory Cells and Ameliorates Adipose Tissue Inflammation and Insulin Resistance. *J Immunol.* 2015;194(10):4777-83.
24. Vasanthakumar A, Moro K, Xin A, Liao Y, Gloury R, Kawamoto S, et al. The transcriptional regulators IRF4, BATF and IL-33 orchestrate development and maintenance of adipose tissue-resident regulatory T cells. *Nat Immunol.* 2015;16(3):276-85.
25. Yamada Y, Nguyen TT, Impellizzeri D, Mineura K, Shibuya R, Gomariz A, et al. Biased IL-2 signals induce Foxp3-rich pulmonary lymphoid structures and facilitate long-term lung allograft acceptance in mice. *Nat Commun.* 2023;14(1):1383.
26. Qin S, Cobbold SP, Pope H, Elliott J, Kioussis D, Davies J, et al. "Infectious" transplantation tolerance. *Science.* 1993;259(5097):974-7.
27. Kendal AR, Chen Y, Regateiro FS, Ma J, Adams E, Cobbold SP, et al. Sustained suppression by Foxp3+ regulatory T cells is vital for infectious transplantation tolerance. *J Exp Med.* 2011;208(10):2043-53.
28. Kolodin D, van Panhuys N, Li C, Magnuson AM, Cipolletta D, Miller CM, et al. Antigen- and cytokine-driven accumulation of regulatory T cells in visceral adipose tissue of lean mice. *Cell Metab.* 2015;21(4):543-57.
29. Feuerer M, Herrero L, Cipolletta D, Naaz A, Wong J, Nayer A, et al. Lean, but not obese, fat is enriched for a unique population of regulatory T cells that affect metabolic parameters. *Nat Med.* 2009;15(8):930-9.
30. Burzyn D, Kuswanto W, Kolodin D, Shadrach JL, Cerletti M, Jang Y, et al. A special population of regulatory T cells potentiates muscle repair. *Cell.* 2013;155(6):1282-95.

31. Niedbala W, Cai B, Liu H, Pitman N, Chang L, and Liew FY. Nitric oxide induces CD4+CD25+ Foxp3 regulatory T cells from CD4+CD25 T cells via p53, IL-2, and OX40. *Proc Natl Acad Sci U S A*. 2007;104(39):15478-83.
32. Wang Z, Hong J, Sun W, Xu G, Li N, Chen X, et al. Role of IFN-gamma in induction of Foxp3 and conversion of CD4+ CD25- T cells to CD4+ Tregs. *J Clin Invest*. 2006;116(9):2434-41.
33. Misumi K, Wheeler DS, Aoki Y, Combs MP, Braeuer RR, Higashikubo R, et al. Humoral immune responses mediate the development of a restrictive phenotype of chronic lung allograft dysfunction. *JCI Insight*. 2020;5(23).
34. Watanabe T, Martinu T, Chruscinski A, Boonstra K, Joe B, Horie M, et al. A B cell-dependent pathway drives chronic lung allograft rejection after ischemia-reperfusion injury in mice. *Am J Transplant*. 2019;19(12):3377-89.
35. Li W, Goldstein DR, Bribriescio AC, Nava RG, Spahn JH, Wang X, et al. Surgical technique for lung retransplantation in the mouse. *J Thorac Dis*. 2013;5(3):321-5.
36. Aguilar PR, Carpenter D, Ritter J, Yusen RD, Witt CA, Byers DE, et al. The role of C4d deposition in the diagnosis of antibody-mediated rejection after lung transplantation. *Am J Transplant*. 2018;18(4):936-44.
37. Clemente-Casares X, Blanco J, Ambalavanan P, Yamanouchi J, Singha S, Fandos C, et al. Expanding antigen-specific regulatory networks to treat autoimmunity. *Nature*. 2016;530(7591):434-40.
38. Miller ML, Daniels MD, Wang T, Chen J, Young J, Xu J, et al. Spontaneous restoration of transplantation tolerance after acute rejection. *Nat Commun*. 2015;6:7566.
39. Jane-Wit D, Manes TD, Yi T, Qin L, Clark P, Kirkiles-Smith NC, et al. Alloantibody and complement promote T cell-mediated cardiac allograft vasculopathy through noncanonical nuclear factor-kappaB signaling in endothelial cells. *Circulation*. 2013;128(23):2504-16.
40. Xie CB, Zhou J, Mackay S, and Pober JS. Complement-activated human endothelial cells stimulate increased polyfunctionality in alloreactive T cells. *Am J Transplant*. 2021;21(5):1902-9.
41. Li C, DiSpirito JR, Zemmour D, Spallanzani RG, Kuswanto W, Benoist C, et al. TCR Transgenic Mice Reveal Stepwise, Multi-site Acquisition of the Distinctive Fat-Treg Phenotype. *Cell*. 2018;174(2):285-99 e12.
42. Menard MT, Schwarze ML, Allan JS, Johnston DR, Mawulawde K, Shimizu A, et al. Composite "thymoheart" transplantation improves cardiac allograft survival. *Am J Transplant*. 2004;4(1):79-86.
43. Yamada K, Shimizu A, Utsugi R, Ierino FL, Gargollo P, Haller GW, et al. Thymic transplantation in miniature swine. II. Induction of tolerance by transplantation of composite thymokidneys to thymectomized recipients. *J Immunol*. 2000;164(6):3079-86.
44. Outtz Reed H, Wang L, Kahn ML, and Hancock WW. Donor-host Lymphatic Anastomosis After Murine Lung Transplantation. *Transplantation*. 2020;104(3):511-5.
45. Pichery M, Mirey E, Mercier P, Lefrancais E, Dujardin A, Ortega N, et al. Endogenous IL-33 is highly expressed in mouse epithelial barrier tissues, lymphoid organs, brain, embryos, and inflamed tissues: in situ analysis using a novel Il-33-LacZ gene trap reporter strain. *J Immunol*. 2012;188(7):3488-95.
46. Sun R, Zhao H, Gao DS, Ni A, Li H, Chen L, et al. Amphiregulin couples IL1RL1(+) regulatory T cells and cancer-associated fibroblasts to impede antitumor immunity. *Sci Adv*. 2023;9(34):eadd7399.

47. Dwyer GK, D'Cruz LM, and Turnquist HR. Emerging Functions of IL-33 in Homeostasis and Immunity. *Annu Rev Immunol.* 2022;40:15-43.
48. Guo Y, Mei Z, Li D, Banerjee A, Khalil MA, Burke A, et al. Ischemia reperfusion injury facilitates lung allograft acceptance through IL-33-mediated activation of donor-derived IL-5 producing group 2 innate lymphoid cells. *Am J Transplant.* 2022;22(8):1963-75.
49. Xie D, Miao W, Xu F, Yuan C, Li S, Wang C, et al. IL-33/ST2 Axis Protects Against Traumatic Brain Injury Through Enhancing the Function of Regulatory T Cells. *Front Immunol.* 2022;13:860772.
50. Ameri AH, Moradi Tuchayi S, Zaalberg A, Park JH, Ngo KH, Li T, et al. IL-33/regulatory T cell axis triggers the development of a tumor-promoting immune environment in chronic inflammation. *Proc Natl Acad Sci U S A.* 2019;116(7):2646-51.
51. Matta BM, Reichenbach DK, Zhang X, Mathews L, Koehn BH, Dwyer GK, et al. Peri-alloHCT IL-33 administration expands recipient T-regulatory cells that protect mice against acute GVHD. *Blood.* 2016;128(3):427-39.
52. Dagher R, Copenhagen AM, Besnard V, Berlin A, Hamidi F, Maret M, et al. IL-33-ST2 axis regulates myeloid cell differentiation and activation enabling effective club cell regeneration. *Nat Commun.* 2020;11(1):4786.
53. Turnquist HR, Zhao Z, Rosborough BR, Liu Q, Castellaneta A, Isse K, et al. IL-33 expands suppressive CD11b⁺ Gr-1(int) and regulatory T cells, including ST2L⁺ Foxp3⁺ cells, and mediates regulatory T cell-dependent promotion of cardiac allograft survival. *J Immunol.* 2011;187(9):4598-610.
54. Kawai K, Uchiyama M, Hester J, and Issa F. IL-33 drives the production of mouse regulatory T cells with enhanced in vivo suppressive activity in skin transplantation. *Am J Transplant.* 2021;21(3):978-92.
55. Li D, Guabiraba R, Besnard AG, Komai-Koma M, Jabir MS, Zhang L, et al. IL-33 promotes ST2-dependent lung fibrosis by the induction of alternatively activated macrophages and innate lymphoid cells in mice. *J Allergy Clin Immunol.* 2014;134(6):1422-32 e11.
56. Prefontaine D, Nadigel J, Chouiali F, Audusseau S, Semlali A, Chakir J, et al. Increased IL-33 expression by epithelial cells in bronchial asthma. *J Allergy Clin Immunol.* 2010;125(3):752-4.
57. Byers DE, Alexander-Brett J, Patel AC, Agapov E, Dang-Vu G, Jin X, et al. Long-term IL-33-producing epithelial progenitor cells in chronic obstructive lung disease. *J Clin Invest.* 2013;123(9):3967-82.
58. Neurohr C, Kneidinger N, Ghiani A, Monforte V, Knoop C, Jaksch P, et al. A randomized controlled trial of liposomal cyclosporine A for inhalation in the prevention of bronchiolitis obliterans syndrome following lung transplantation. *Am J Transplant.* 2022;22(1):222-9.
59. Terada Y, Li W, Shepherd HM, Takahashi T, Yokoyama Y, Bery AI, et al. Smoking exposure-induced bronchus-associated lymphoid tissue in donor lungs does not prevent tolerance induction after transplantation. *Am J Transplant.* 2023.
60. Wang L, Wang Z, Han R, Samanta A, Ge G, Levin LS, et al. Donor bone-marrow CXCR4⁺ Foxp3⁺ T-regulatory cells are essential for costimulation blockade-induced long-term survival of murine limb transplants. *Sci Rep.* 2020;10(1):9292.
61. Dilek N, Poirier N, Usal C, Martinet B, Blancho G, and Vanhove B. Control of transplant tolerance and intragraft regulatory T cell localization by myeloid-derived suppressor cells and CCL5. *J Immunol.* 2012;188(9):4209-16.

62. Montane J, Obach M, Alvarez S, Bischoff L, Dai DL, Soukhatcheva G, et al. CCL22 Prevents Rejection of Mouse Islet Allografts and Induces Donor-Specific Tolerance. *Cell Transplant*. 2015;24(10):2143-54.
63. Florentin J, Zhao J, Tai YY, Sun W, Ohayon LL, O'Neil SP, et al. Loss of Amphiregulin drives inflammation and endothelial apoptosis in pulmonary hypertension. *Life Sci Alliance*. 2022;5(11).
64. Arpaia N, Green JA, Moltedo B, Arvey A, Hemmers S, Yuan S, et al. A Distinct Function of Regulatory T Cells in Tissue Protection. *Cell*. 2015;162(5):1078-89.
65. Zaiss DM, van Loosdregt J, Gorlani A, Bekker CP, Grone A, Sibilina M, et al. Amphiregulin enhances regulatory T cell-suppressive function via the epidermal growth factor receptor. *Immunity*. 2013;38(2):275-84.
66. Wang S, Zhang Y, Wang Y, Ye P, Li J, Li H, et al. Amphiregulin Confers Regulatory T Cell Suppressive Function and Tumor Invasion via the EGFR/GSK-3beta/Foxp3 Axis. *J Biol Chem*. 2016;291(40):21085-95.
67. Okazaki M, Krupnick AS, Kornfeld CG, Lai JM, Ritter JH, Richardson SB, et al. A mouse model of orthotopic vascularized aerated lung transplantation. *Am J Transplant*. 2007;7(6):1672-9.
68. Li W, Shepherd HM, Terada Y, Shay AE, Bery AI, Gelman AE, et al. Resolvin D1 prevents injurious neutrophil swarming in transplanted lungs. *Proc Natl Acad Sci U S A*. 2023;120(31):e2302938120.
69. Osorio D, and Cai JJ. Systematic determination of the mitochondrial proportion in human and mice tissues for single-cell RNA-sequencing data quality control. *Bioinformatics*. 2021;37(7):963-7.
70. Hafemeister C, and Satija R. Normalization and variance stabilization of single-cell RNA-seq data using regularized negative binomial regression. *Genome Biol*. 2019;20(1):296.
71. Korsunsky I, Millard N, Fan J, Slowikowski K, Zhang F, Wei K, et al. Fast, sensitive and accurate integration of single-cell data with Harmony. *Nat Methods*. 2019;16(12):1289-96.

Figures

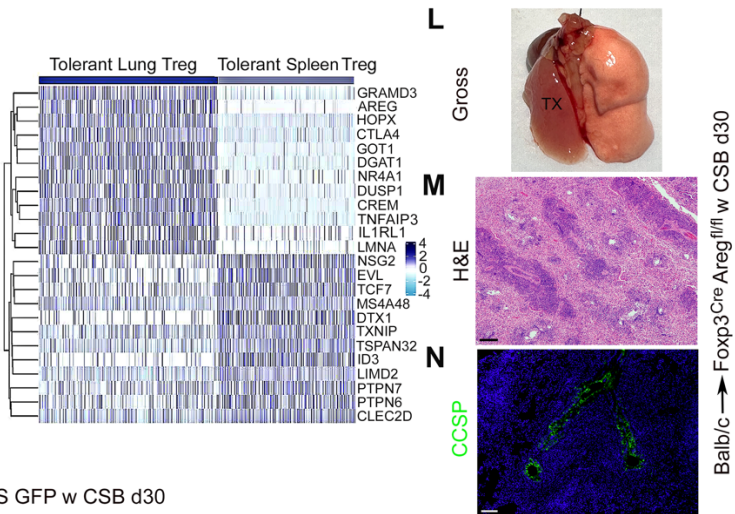
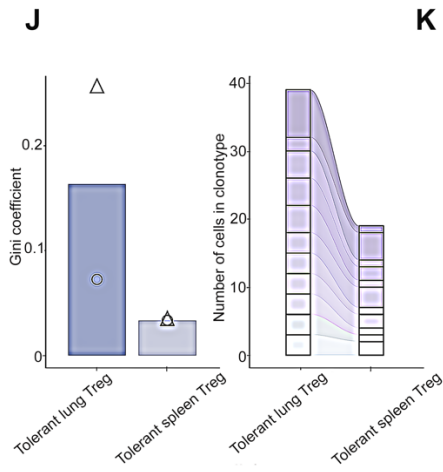
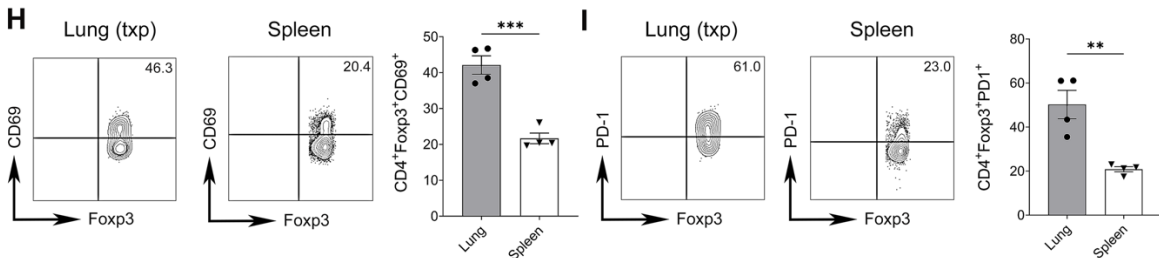
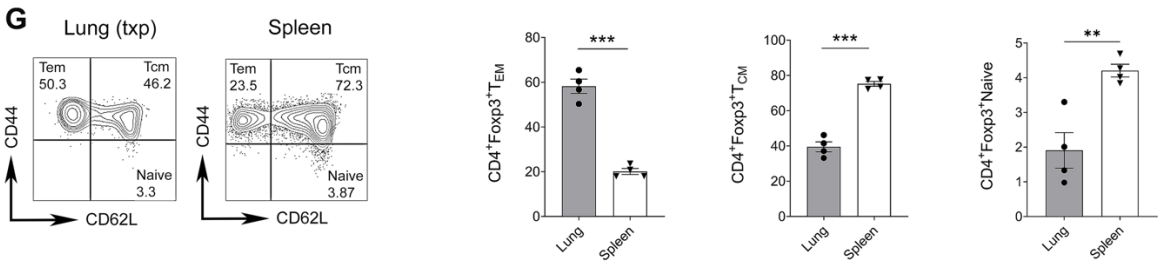
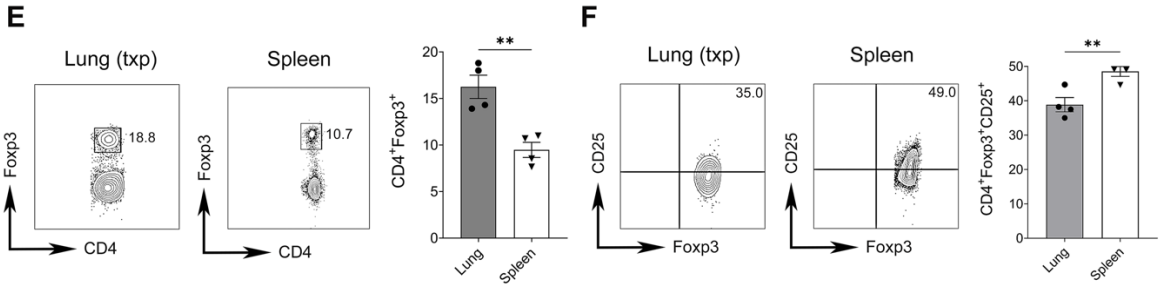
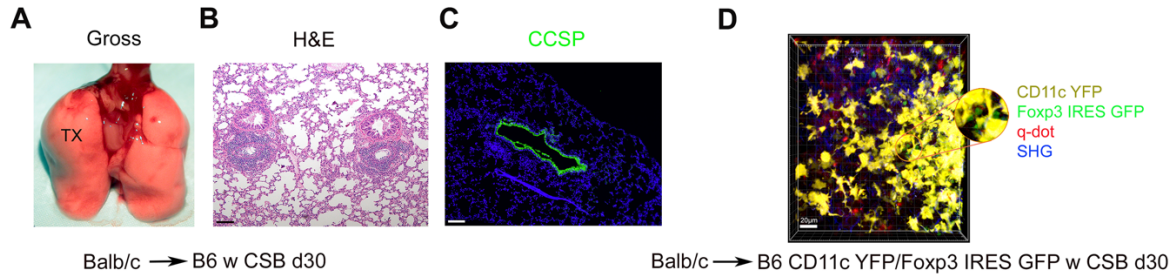


Figure 1. Allograft-resident and spleen Foxp3⁺ cells are phenotypically and transcriptionally distinct in tolerant lung transplant recipients. **A.** Gross image (n=6), **B.** H&E staining (n=6), and **C.** CCSP immunofluorescence staining (n=2) of left lung transplant from Balb/c donor into CSB-treated B6 recipient, at least 30 days after engraftment. **D.** Two-photon intravital microscopy of Balb/c lung at least 30 days after transplantation into CSB-treated B6 CD11c-EYFP/Foxp3-GFP recipient (n=3, scale bar 20 μ m). CD11c⁺ cells are yellow, Foxp3⁺ cells are green, collagen appears blue due to second harmonic generation and vessels are red following intravenous injection of quantum dots. Representative flow cytometry plots and quantification of abundance of **E.** Foxp3-expressing CD45⁺CD90.2⁺CD4⁺CD8⁻ T cells, **F.** CD25-expressing CD45⁺CD90.2⁺CD4⁺CD8⁻Foxp3⁺ T cells (CD25 expression determined based on isotype control staining), **G.** effector memory (CD44^{hi}CD62L^{lo}), central memory (CD44^{hi}CD62L^{hi}), and naïve (CD44^{lo}CD62L^{hi}) CD45⁺CD90.2⁺CD4⁺CD8⁻Foxp3⁺ T cells, **H.** CD69-expressing CD45⁺CD90.2⁺CD4⁺CD8⁻Foxp3⁺ T cells and **I.** PD-1-expressing CD45⁺CD90.2⁺CD4⁺CD8⁻Foxp3⁺ T cells in Balb/c lung and recipient spleen at least 30 days after transplantation into CSB-treated B6 recipients (n=4). At least 30 days after transplantation of Balb/c lungs into CSB-treated B6 Foxp3-GFP mice, CD45⁺CD90.2⁺CD4⁺CD8⁻GFP⁺ cells were sorted and processed for TCR and genome sequencing (n=2). **J.** Gini coefficient (0 represents maximal diversity) comparison of clonal expansion (left) and number of cells in the top eleven shared clonotypes between Foxp3⁺ cells in tolerant lung allografts and recipient spleens (right) (symbols (Δ ;O) denote individual mice). **K.** Heatmap of most highly differentially expressed genes in Foxp3⁺ cells between tolerant lung allografts and recipient spleens (2 pooled lungs and spleens). **L.** Gross image (n=4), **M.** H&E staining (n=4), and **N.** CCSP immunofluorescence staining (n=2) of Balb/c lungs 30 days after transplantation into CSB-treated B6 Foxp3-YFP-Cre *Areg*^{fl/fl} mice. Results expressed as mean \pm SEM. Scale bars represent 100 μ m, unless otherwise specified. ** p<0.01, *** p<0.001. (d30 = day 30, TX = transplanted lung, H&E = hematoxylin and eosin, CCSP = club cell secretory protein, CSB = costimulatory blockade, YFP = yellow fluorescent protein, GFP = green fluorescent protein, SHG = secondary harmonic generation, q-dot = quantum dot, T_{EM} = T effector memory, T_{CM} = T central memory, Treg = regulatory Foxp3⁺ T cell)

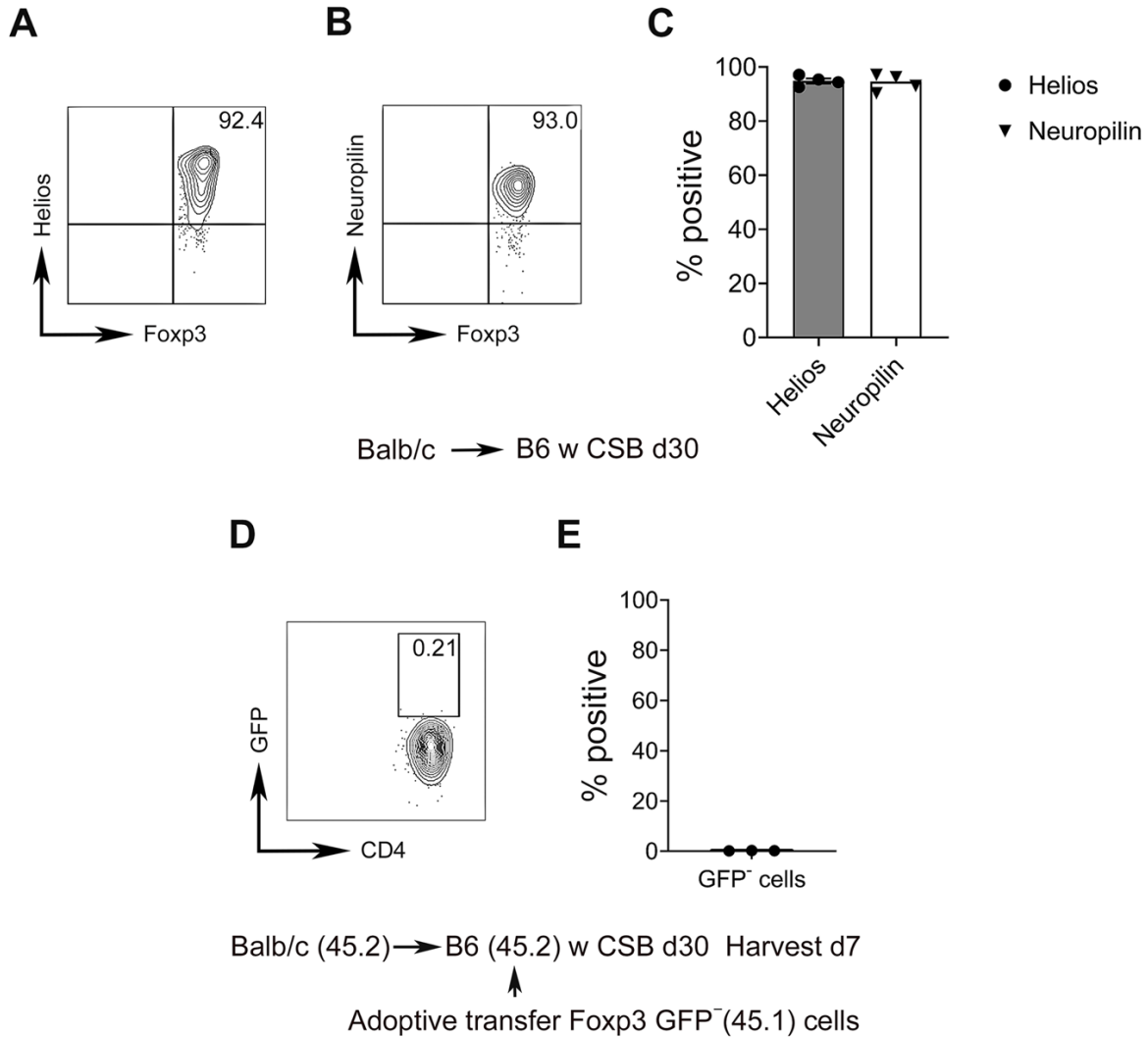


Figure 2. Graft-infiltrating Foxp3⁺ cells are derived from the thymus rather than from peripheral conversion of Foxp3⁻ T cells. Representative flow cytometric plots (**A**, **B**) and quantification (**C**) of Helios and Neuropilin-1 expression by CD45⁺CD90.2⁺CD4⁺CD8⁻Foxp3⁺ T cells in Balb/c lungs at least 30 days after transplantation into CSB-treated B6 recipients (n=4). Thirty days following transplantation of Balb/c (CD45.2) lungs into CSB-treated B6 (CD45.2) recipients, CD90.2⁺CD4⁺GFP⁻ T cells, isolated from secondary lymphoid organs of B6 Foxp3-GFP (CD45.1) reporter mice, were injected intravenously. Lungs were analyzed 7 days later. **D**, **E**. Representative flow cytometric plot and analysis of GFP expression in adoptively transferred cells (CD45.1⁺) in lung allografts (n=3). Results expressed as mean ± SEM. (d = day, CSB = costimulatory blockade, GFP = green-fluorescent protein)

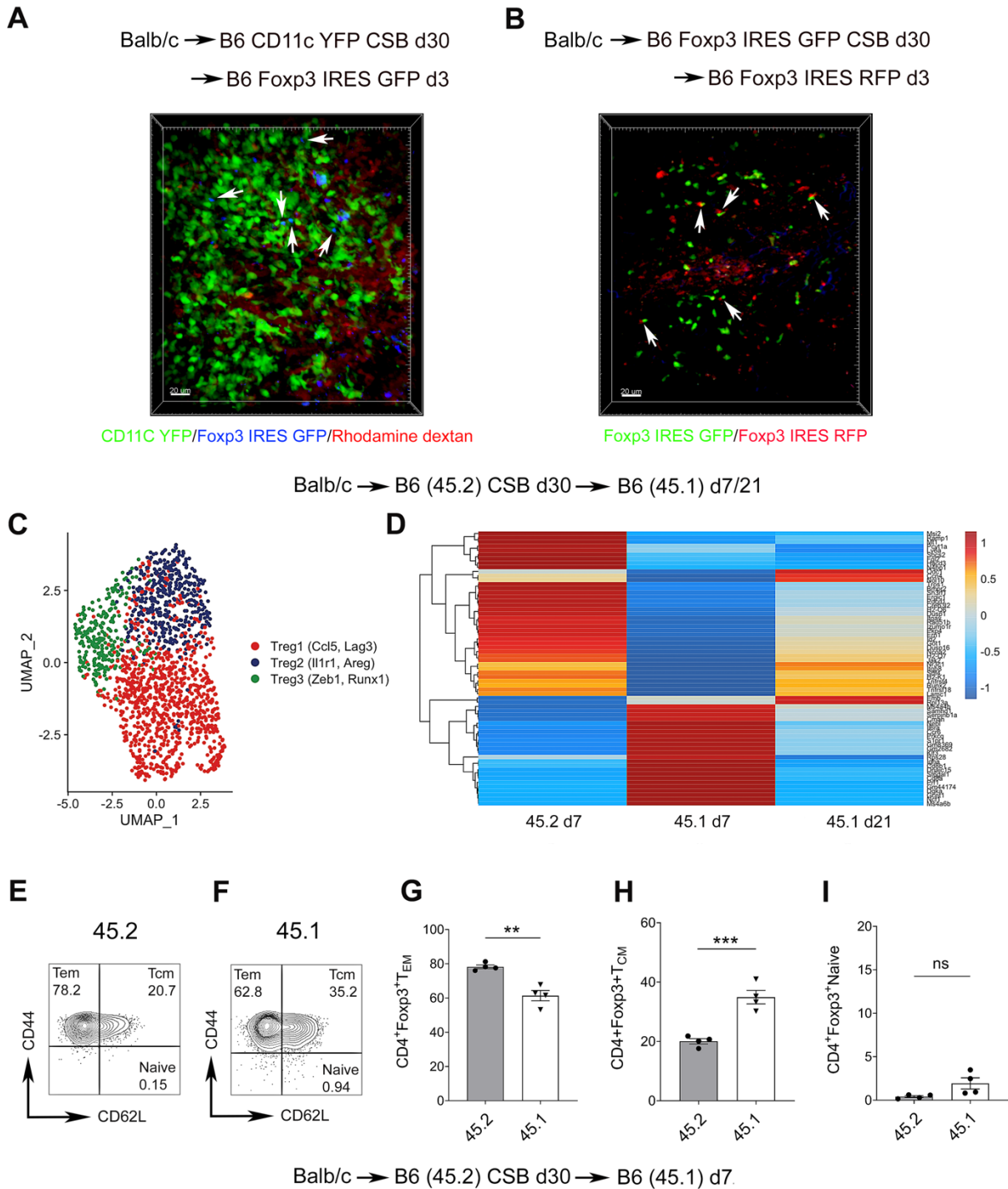


Figure 3. Newly recruited Foxp3⁺ cells infiltrate BALT within tolerant lung allografts and differ transcriptionally from graft-resident Foxp3⁺ cells. **A.** Balb/c lungs, initially transplanted into CSB-treated B6 CD11c-EYFP mice and then at least 30 days later re-transplanted into non-immunosuppressed B6 Foxp3-GFP hosts were imaged with intravital two-photon microscopy three days after re-transplantation (n=3). White arrows point to contacts between Foxp3⁺ (blue) and CD11c⁺ (green) cells within the BALT of lung allografts. Rhodamine dextran labels vessels red. **B.** Balb/c lungs, initially transplanted into CSB-treated B6 Foxp3-GFP mice and then at least

30 days later re-transplanted into non-immunosuppressed B6 Foxp3-RFP recipients were imaged with intravital two-photon microscopy three days after re-transplantation (n=3). White arrows point to contacts between graft-resident (green) and graft-infiltrating (red) Foxp3⁺ cells within lung allografts. Balb/c (CD45.2) lungs were transplanted into CSB-treated B6 (CD45.2) recipients and at least 30 days later re-transplanted into non-immunosuppressed B6 (CD45.1) mice. Seven and 21 days after re-transplantation, graft-resident (CD45.2) (7 days) and extravasated graft-infiltrating (CD45.1) (7 and 21 days) T cells were sorted from the lung allografts (samples were collected from 4 re-transplant recipients and pooled) and processed for single cell RNA sequencing (**C, D**). **C.** UMAP embedding plot of regulatory T cell subpopulations. **D.** Heatmap of statistically significant ($\log_2FC > 0.25$, adjusted p-value < 0.05) differentially expressed genes between graft-resident CD45.2 (day 7) and extravasated graft-infiltrating CD45.1 (days 7 and 21) regulatory T cells grouped by condition. **E.-I.** Representative flow cytometry plots and quantification of abundance of effector memory (CD44^{hi}CD62L^{lo}), central memory (CD44^{hi}CD62L^{hi}), and naïve (CD44^{lo}CD62L^{hi}) graft-resident CD45.2⁺ versus graft-infiltrating CD45.1⁺ CD90.2⁺CD4⁺CD8⁻Foxp3⁺ T cells on day 7 (n=4). Results expressed as mean \pm SEM. Scale bars 20 μ m. ** p<0.01, ***p<0.001. (d= day, CSB = costimulatory blockade, YFP = yellow fluorescent protein, GFP = green fluorescent protein, RFP = red fluorescent protein, UMAP = uniform manifestation approximation and projection, T_{EM} = T effector memory, T_{CM} = T central memory, ns = not significant)

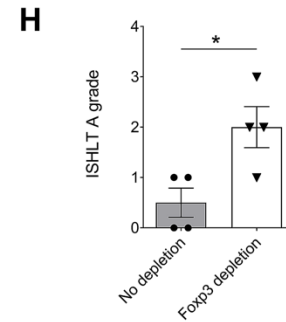
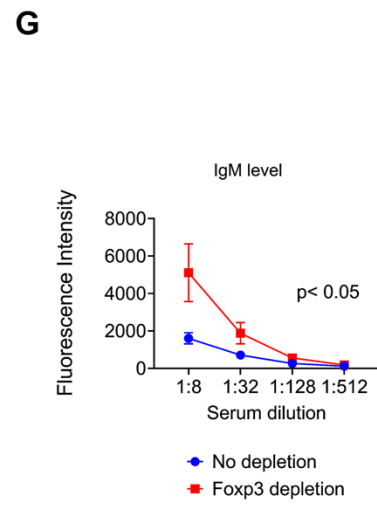
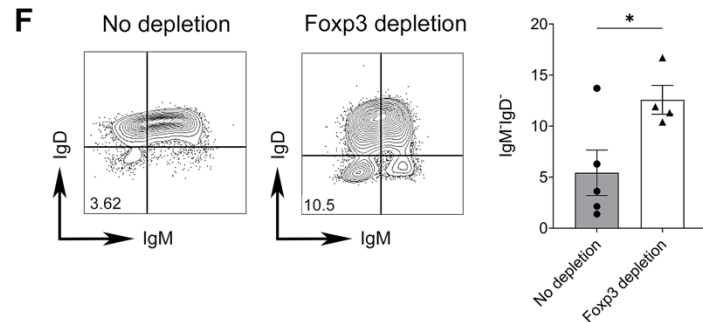
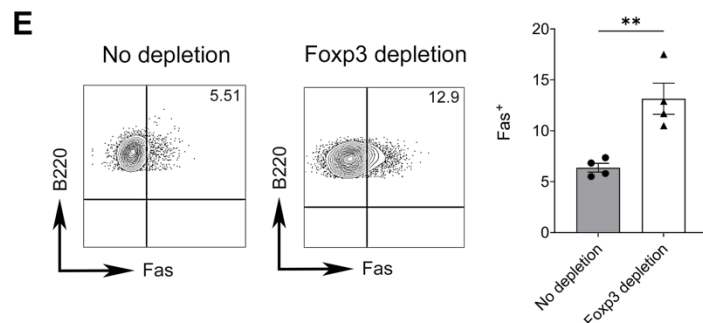
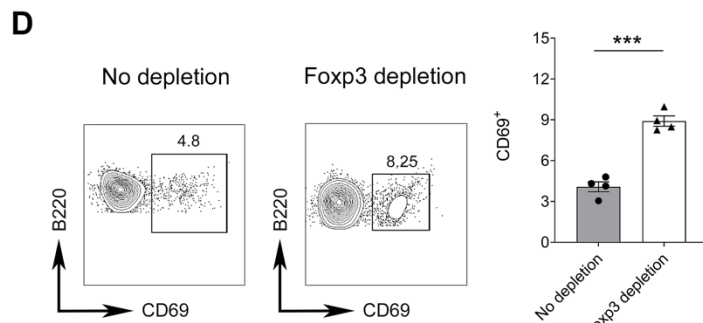
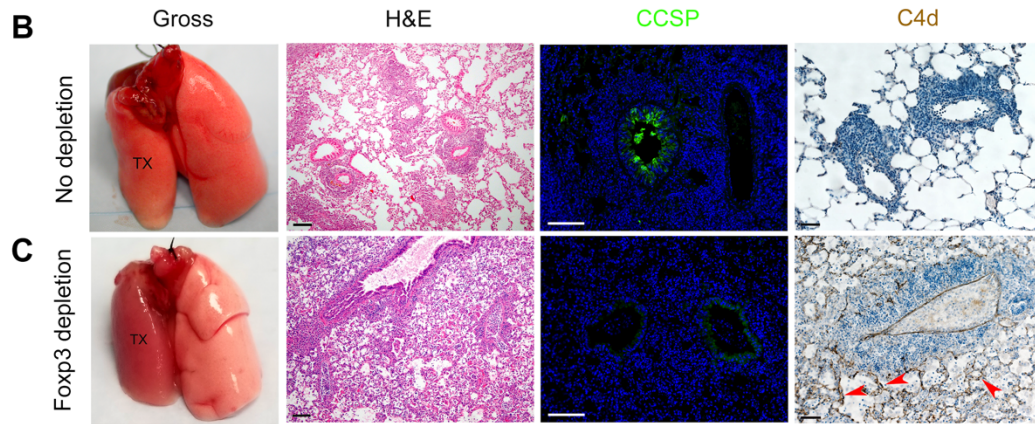
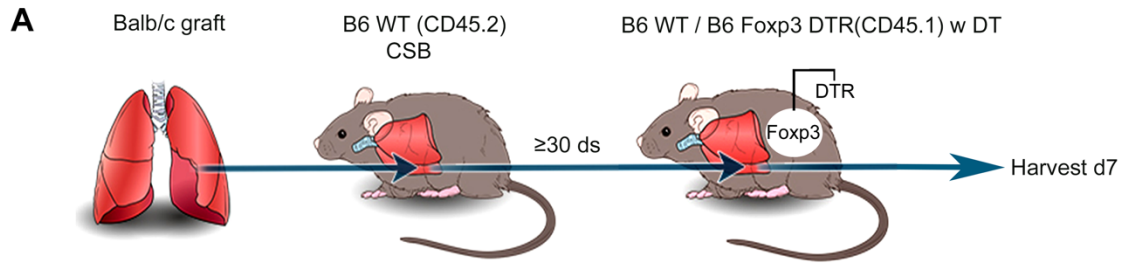


Figure 4. Depletion of recipient Foxp3⁺ cells results in loss of allograft tolerance. **A.** Schematic depicting left lung from Balb/c (CD45.2) donor initially transplanted into CSB-treated B6 (CD45.2) primary recipient and then ≥ 30 days later re-transplanted into non-immunosuppressed B6 (CD45.1) or B6 Foxp3-DTR (CD45.1) secondary recipient, with diphtheria toxin (DT) administration and analysis seven days after re-transplantation. Gross image (first panel, n=4), H&E histology (second panel, n=4), CCSP immunofluorescence staining (green, third panel, n=2), and immunohistochemical staining for C4d (brown, fourth panel, arrows pointing to alveolar endothelial C4d staining, n=2) in DT-treated **B.** B6 and **C.** B6 Foxp3-DTR secondary recipients. Representative flow cytometric plots and quantification of abundance of **D.** CD69 **E.** Fas **F.** and IgM/IgD expression in graft-infiltrating CD45.2⁻CD45.1⁺CD19⁺B220⁺ B cells in control (left panels) and recipient Foxp3-depleted (right panels) re-transplants (n ≥ 4). **G.** Flow cytometric analysis of serum donor-specific IgM antibody titers (expressed as mean fluorescence intensity) and **H.** ISHLT A rejection grades in control and recipient Foxp3-depleted re-transplants (n=4). Results expressed as mean \pm SEM. Scale bars represent 100 μ m. *p<0.05, **p<0.01, ***p<0.001. (WT = wildtype, CSB = costimulatory blockade, d=days, DTR = diphtheria toxin receptor, DT = diphtheria toxin, H&E = hematoxylin and eosin, CCSP = club cell secretory protein, C4d = complement 4d, TX = transplanted lung)

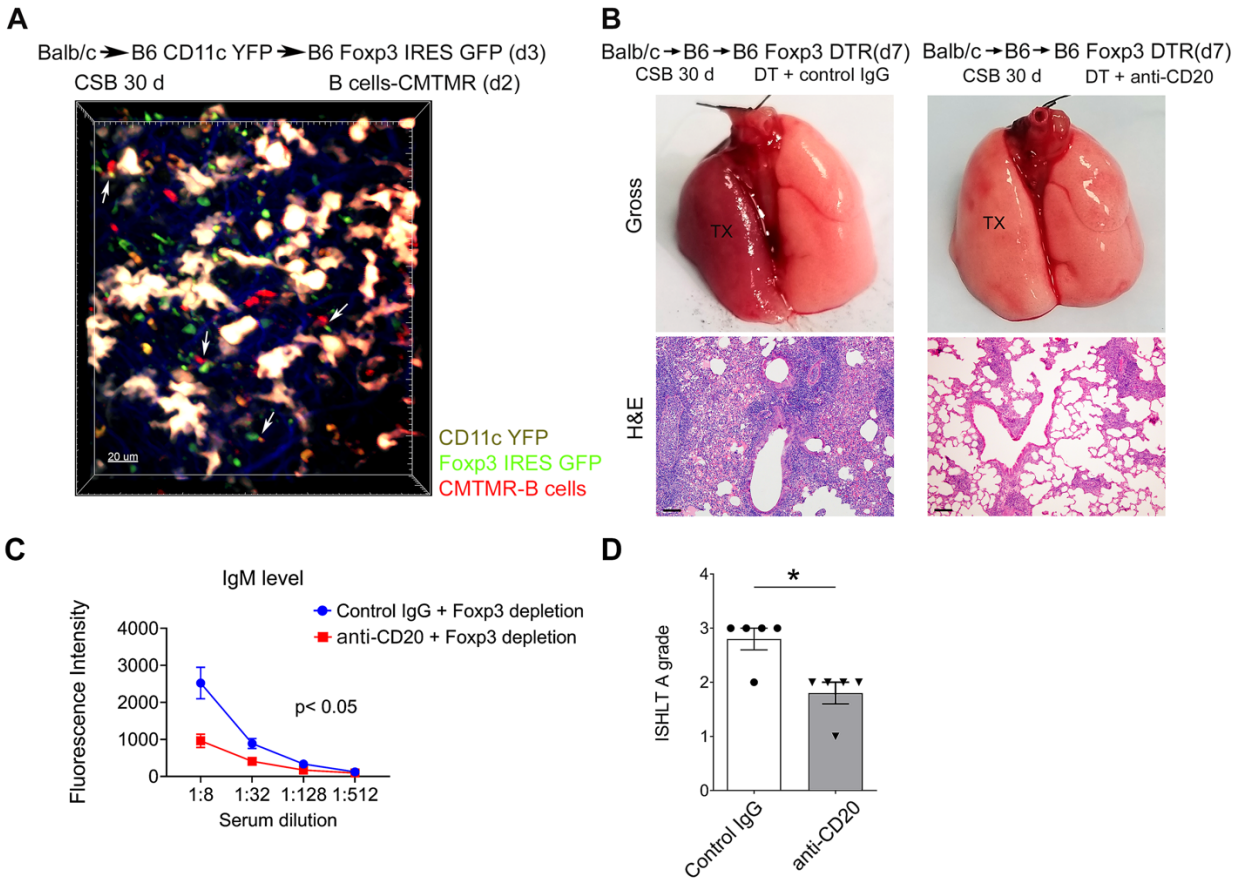


Figure 5. Rejection after recipient Foxp3⁺ cell depletion is dependent on B cells. **A.** Balb/c lungs were initially transplanted into CSB-treated B6 CD11c-EYFP mice and then re-transplanted into non-immunosuppressed B6 Foxp3-GFP hosts at least 30 days later. Recipient-matched B6 CMTMR-labeled B cells were injected into recipients two days after re-transplantation and allografts were imaged with intravital two-photon microscopy the following day (n=3). White arrows point to contacts between Foxp3⁺ (green) and B cells (red). CD11c⁺ cells (yellow) mark the BALT within tolerant lung allografts (n=4). Scale bar 20 μ m. **B.** Gross (top) and histological (H&E) (bottom) images of Balb/c lungs that were initially transplanted into CSB-treated B6 mice and then at least 30 days later re-transplanted into Foxp3-depleted non-immunosuppressed B6 recipients that received anti-CD20 (right) or isotype control antibodies (left). Scale bar represents 100 μ m. **C.** Flow cytometric analysis of serum IgM DSA titers (expressed as mean fluorescence intensity) and **D.** ISHLT A rejection grades in re-transplant recipients described in **B** (n \geq 4). (CSB = costimulatory blockade, YFP = yellow fluorescent protein, GFP = green fluorescent protein, CMTMR = rhodamine-based red cell dye, H&E = hematoxylin and eosin, d = days, DT = diphtheria toxin, DTR = diphtheria toxin receptor, TX = transplanted lung)

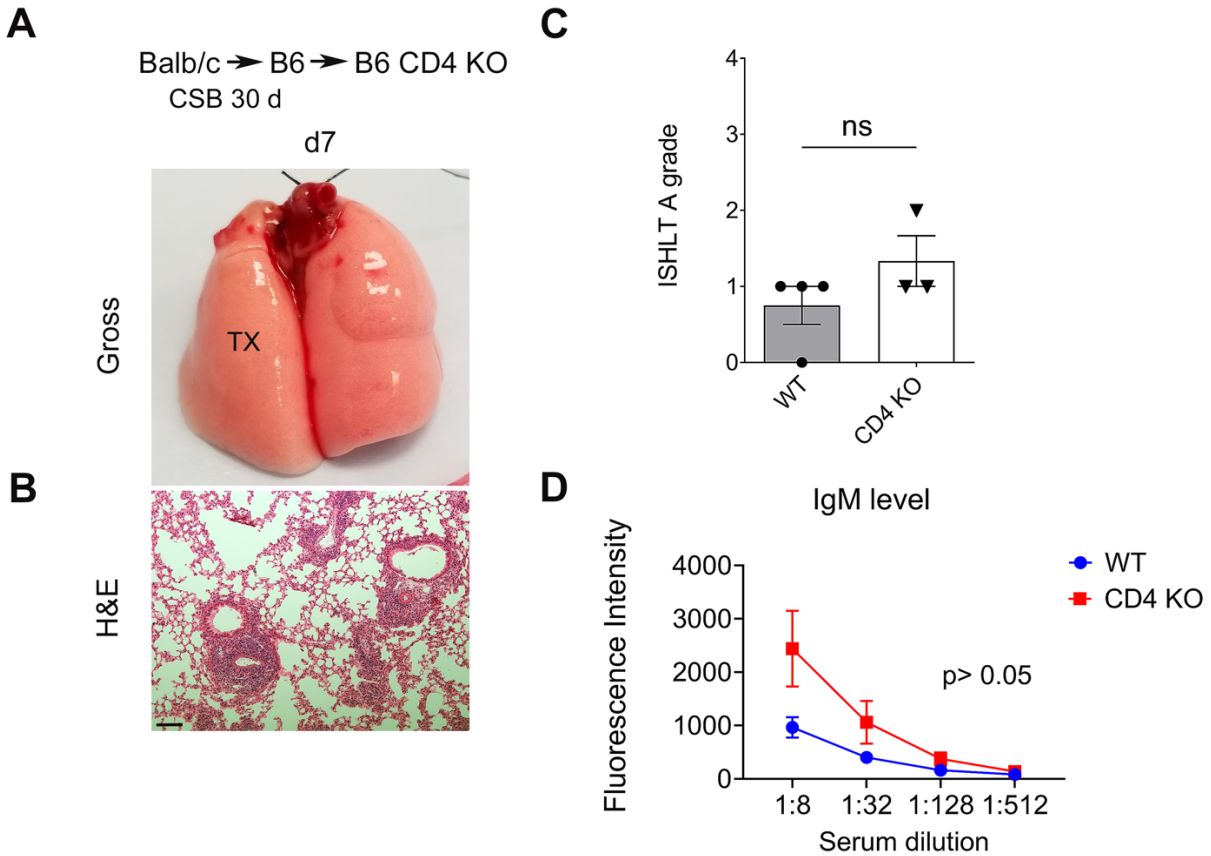


Figure 6. Lung allograft tolerance is maintained in the global absence of CD4⁺ T cells. **A.** Gross and **B.** histological (H&E) images of Balb/c lungs that were initially transplanted into CSB-treated B6 mice and then at least 30 days later re-transplanted into non-immunosuppressed B6 CD4 knockout recipients. Scale bar 100 μ m. **C.** ISHLT A rejection grades and **D.** flow cytometric analysis of serum IgM DSA titers (expressed as mean fluorescence intensity) in re-transplants depicted in **A, B** compared with tolerant Balb/c lung allografts that were re-transplanted into non-immunosuppressed B6 mice ($n \geq 3$). Mice were examined seven days after re-transplantation (CSB = costimulatory blockade, d = days, KO = knockout, TX = transplanted lung, H&E = hematoxylin and eosin, CTRL = control)

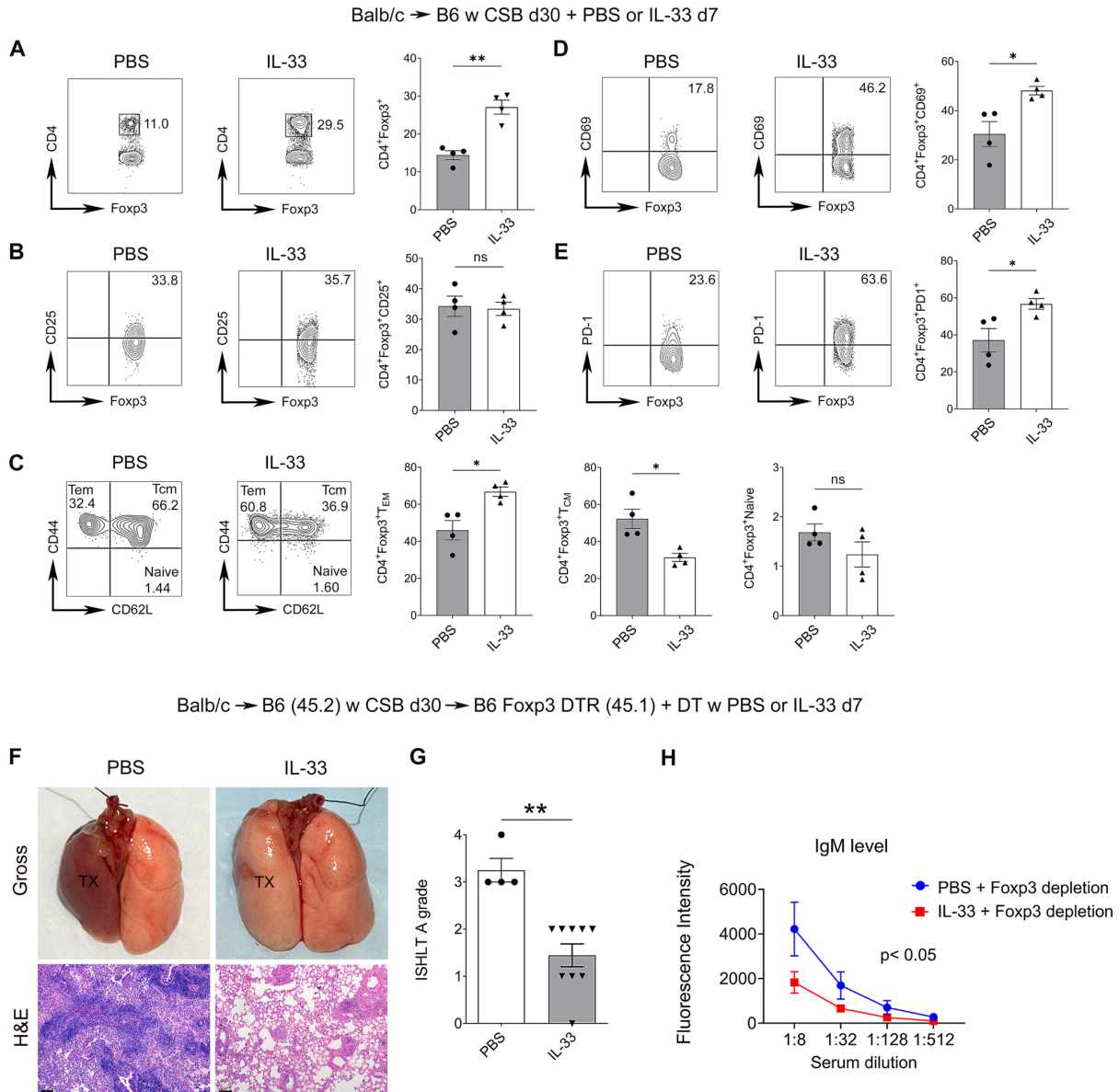


Figure 7. IL-33 promotes the expansion and activation of lung allograft-resident Foxp3⁺ cells. Balb/c lungs were transplanted into CSB-treated B6 recipients. At least 30 days after transplantation, recipients were treated with intratracheal IL-33 or PBS and grafts were analyzed 7 days later. Representative flow cytometry plots and quantification of abundance of **A.** Foxp3-expressing CD45⁺CD90.2⁺CD4⁺CD8⁻ T cells, **B.** CD25-expressing CD45⁺CD90.2⁺CD4⁺CD8⁻ Foxp3⁺ T cells, **C.** effector memory (CD44^{hi}CD62L^{lo}), central memory (CD44^{hi}CD62L^{hi}), and naïve (CD44^{lo}CD62L^{hi}) CD45⁺CD90.2⁺CD4⁺CD8⁻Foxp3⁺ T cells, **D.** CD69-expressing CD45⁺CD90.2⁺CD4⁺CD8⁻Foxp3⁺ T cells and **E.** PD-1-expressing CD45⁺CD90.2⁺CD4⁺CD8⁻ Foxp3⁺ T cells in lung allografts after treatment with IL-33 or PBS (n=4). **F.** Gross (top) and histological (H&E) (bottom) appearances of left Balb/c lungs that were initially transplanted into CSB-treated B6 recipients and then 30 days later re-transplanted into DT-treated B6 Foxp3-DTR secondary recipients, that received PBS (left, n=4) or IL-33 (right, n=9) intratracheally. Grafts were examined 7 days after re-transplantation. Scale bar 100 μm. **G.** ISHLT A rejection grades

and **H.** flow cytometric analysis of serum IgM DSA titers (expressed as mean fluorescence intensity) in recipients depicted in **F** (PBS n=4; IL-33 n=9). Results expressed as mean \pm SEM. *p<0.05, **p<0.01. (CSB = costimulatory blockade, d = day, PBS = phosphate-buffered saline, T_{EM} = T effector memory, T_{CM} = T central memory, DTR = diphtheria toxin receptor, DT = diphtheria toxin, TX = transplanted lung, H&E = hematoxylin and eosin, ns = not significant)